Computer Microvision Measurements of Stapedial Motion in Human Temporal Bone

by

Bryan Clifford Bilyeu

Submitted to the Department of Electrical Engineering and Computer Science in partial fulfillment of the requirements for the degrees of

Bachelor of Science and

Master of Engineering

at the

MASSACHUSETTS INSTITUTE OF TECHNOLOGY

May 21, 1998

Author .....
Electrical Engineering and Computer Science
May 21, 1998

Certified by .....
Dennis M. Freeman
Assistant Professor of Electrical Engineering
Thesis Supervisor

Accepted by .....
Arthur C. Smith
Chair, Department Committee on Graduate Theses

Computer Microvision Measurements of Stapedial Motion in Human Temporal Bone

by

Bryan Clifford Bilyeu

Submitted to the Department of Electrical Engineering and Computer Science on May 21, 1998, in partial fulfillment of the requirements for the degrees of Bachelor of Science and Master of Engineering in Electrical Engineering and Computer Science.

Abstract

Scientists have marveled at the middle ear for centuries. The importance of the middle ear to hearing and the ease which with it may be damaged make an understanding of this system relevant to clinicians. The middle ear functions as a transformer, in which the motion of the stapes is the output and the sound pressure at the tympanic membrane is the input. Though much studied, the relationship between the motion of those two structures has not been well established. Factors such as access to the human middle ear and the ability to resolve three-dimensional modes of motion have impeded progress.

While there remains no current method of viewing stapes motion in live humans, a new measurement system promises to quantify more accurately small-scale, three-dimensional motions. Computer microvision is a measurement system which uses computer vision algorithms to estimate motions from stroboscopically illuminated digital images taken through a light microscope. The purpose of this thesis is to apply this system to the sound-induced motions of the stapes in a cadaveric human temporal bone preparation. Results of this application contribute more evidence toward a full characterization of the nature of human stapes motion.

Making computer microvision measurements in a range of frequencies from 250 Hz to 6 kHz, I found that stapes motion relative to sound pressure at the tympanic membrane was compliance dominated for frequencies below 800 Hz and achieved resonance at 1.1 kHz. Measurements on the same temporal bone were performed on two separate occasions, and the measurements were repeatable to a factor of two, which is within the range of variation that could be attributed to the condition of the bone. The results show that the stapes translated along some axis, but it was difficult to place that axis in a physiologic frame of reference.

Dennis M. Freeman
Assistant Professor

Acknowledgments

I would first like to thank John Rosowski for his invaluable contribution to this thesis. He spent numerous hours teaching me the rudiments of ear function and otological terminology, forcing me to explain what I had learned of computer microvision, and setting up the temporal bone. I am most grateful for his telling me when my interpretations were colossally dumb and showing me why, his reading and commenting on any draft I sent his way, and his general encouragement.

I also thank Prof. Freeman for his input on my writing and for giving me the chance to do this project. A. J. Aranyosi–troubleshooter extraordinaire–introduced me to computer microvision and was always available to answer my questions about it.

Much of what I have learned at MIT has had little to do with what is taught in the classroom. Iota Mu of Phi Gamma Delta has taught me a good deal about life, especially in this past year. In five years of singing with the MIT Cross Products, I learned a lot about music, the voice, and about working as a team. And I became a tenor.

I thank my parents for putting up with my antics for eighteen years and then footing most of the bill to send me to school. My weekly phone calls home have been key to keeping me sane.

Finally, I thank my Lord and Savior Jesus Christ, without whom neither the hearing ear nor anyone's study of it would be possible. In his infinite patience, he has not only tolerated but loved me, and though I am far from deserving, he has seen fit to shower me with innumerable gifts, including a loving family, dear friends, and a decent education. Most importantly, his grace alone saved me. He loves me, forgives me, and continues to work change in me from the inside out: teaching me, among other things, to rely on his strength and not my own.

"That is why, for Christ's sake, I delight in weaknesses, in insults, in hardships, in persecutions, in difficulties. For when I am weak, then I am strong."

II Corinthians 12:10 (NIV)

Table of Contents

List of Figures

Chapter 1

Introduction

The human ear is an acutely sensitive apparatus. At the threshold of hearing, the air vibrations we perceive as sound are smaller than one atomic diameter. This senstivity arises in part from the inner ear, which is sensitive to vibrations of its input that are also smaller than one atomic diameter. The inner ear, however, is filled with a liquid, and the pressures required to displace a liquid are generally orders of magnitude greater than those needed to displace molecules of a gas. Yet displacements of the stapes–the third bone of the middle ear and the input to the inner ear–are as large as the air vibrations that cause them. Such effectiveness is due to the middle ear–a controlled transformer in function–that collects energy from the acoustic wave that strikes the tympanic membrane and converts it to mechanical energy that excites the inner ear as motion of the stapes.

Although the middle ear is effective in normal hearing individuals, its function is compromised by many clinically improvable conditions. Otitis media–or childhood ear infection–is the most common reason for a child to be taken to a physician. Ear trauma can cause ossicular discontinuity, a disconnection of the bones of the middle ear, or tympanic perforations. Otosclerosis is a bony overgrowth near the footplate of the stapes.

Despite that clinicians routinely treat these conditions, there remain basic questions as to how the middle ear functions in normal individuals. For instance, the mode of stapes motion is not well established: whether it moves as a piston or rocks in some fashion.

The stapes is considered an accurate indicator of the output of the middle ear, and the tympanic membrane is the indicator of the input. While accurate measurements of sound-induced tympanic membrane motions in live humans have long been possible, such is not

the case with the stapes. Because it is encased in bone, the middle ear of healthy patients remains inaccessible to researchers. The low amplitude of stapedial motion at normal, physiological sound pressure levels further complicates the characterization of stapedial motion.

Computer microvision–a measurement system recently developed at the Massachusetts Institute of Technology–provides an answer to the difficulty of measuring small motions. The system has the ability to measure three-dimensional, rigid-body translations to an accuracy of nanometers. The purpose of this thesis is to explore the application of computer microvision to a new target–the cadaveric human stapes–and to present some preliminary results.

1.1 The Anatomy of the Middle Ear

An elementary knowledge of middle ear anatomy and terminology is essential to understanding stapedial motion and its relevance to hearing.

The human ear has three physiologically distinct regions: the outer ear, which collects and focuses sound from the external environment; the middle ear, which converts acoustical energy to mechanical energy; and the inner ear, which converts mechanical energy into nerve signals.

The pinna, the fleshy, outer part of the ear, channels sound down the external auditory canal toward the tympanic membrane or ear drum. The tympanic membrane separates the outside world from the tympanic cavity or middle ear. Figure 1.1 is a sketch of the middle ear which illustrates the spatial relationships between the tympanic membrane, the bones of the middle ear, and the inner ear. The shaded area surrounding the middle ear is the portion of the skull known as the temporal bone.

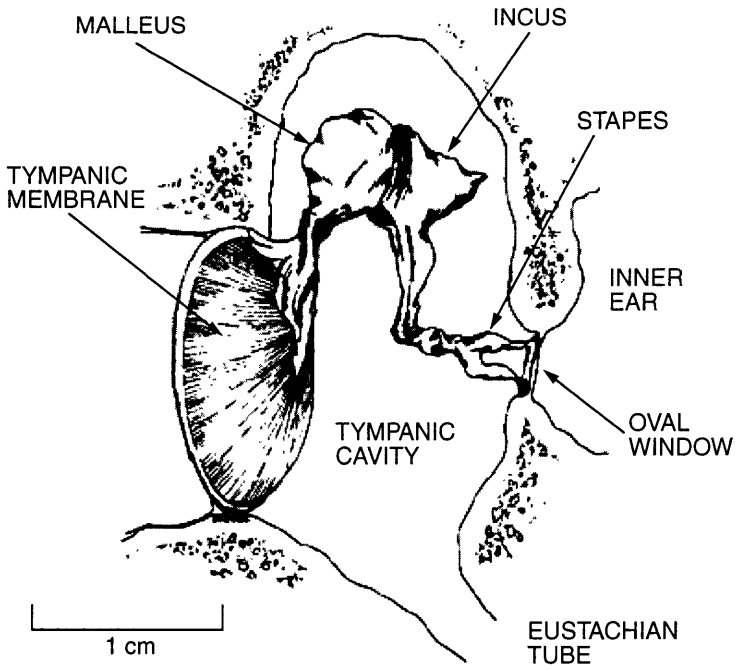

Figure 1.1: The human middle ear. Sketch obtained from Cece (1997).

Static pressure in the middle ear is controlled by the Eustachian tube, which connects the middle ear to the back of the throat. The tympanic membrane converts sound pressure energy into mechanical energy of the ossicles, the three connected bones of the middle ear. Specifically, the first ossicle, the malleus (latin for "hammer"), is attached to the tympanic membrane. It transfers motion to the incus (latin for "anvil"), which in turn transfers motion to the stapes (latin for "stirrup"). The footplate of the stapes is attached to the oval window, the membrane securing the entrance to the cochlea. The cochlea is the conch-shaped, fluid-filled, bony structure of the inner ear. It houses the organ of Corti, which is responsible for converting sound-induced motions into the neural signals that are interpreted by the brain. The stapes, then, directly applies the input to the inner ear. Figure 1.2 is a sketch outlining the general structure of the stapes.

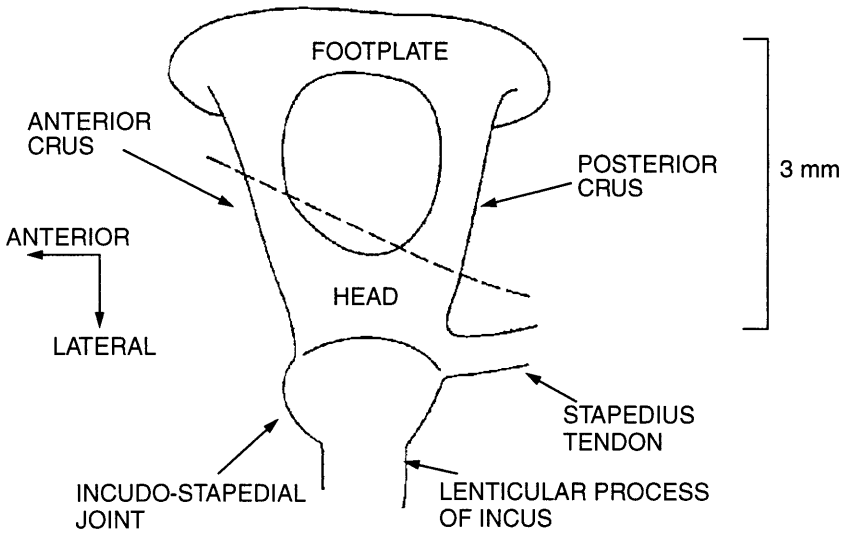

Figure 1.2: The stapes[1]. The portion of the sketch below the dotted line corresponds to the portion of the stapes typically in view in a human temporal bone preparation.

The stapes consists of a head, two crura, and a footplate. The length of the human stapes from head to footplate is approximately 3 mm. The head of the stapes is connected through the incudo-stapedial joint to the lenticular process of the incus. Attached to the stapes head is the stapedius tendon, which connects the stapes and the stapedius muscle. Contraction of the stapedius muscle can control the stiffness of the ossicular chain, affecting the transmission characteristics of the middle ear.

1.2 Measurements of and Theories on Stapes Motion

For centuries, researchers have sought to understand the mechanical properties of the middle ear and their significance to human hearing. Because of the infeasibility of making direct measurements on live humans, experimenters have used various test subjects, including live cats and human cadavers. The measurements have also been made employ-

1. Based on a sketch of the feline stapes from Guinan and Peake .

ing various methods. Some researchers have used methods such as electromagnetic pick-ups or capacitive probes to measure ossicular motion, while others have used laser doppler vibrometers or made estimates with the human eye assisted by light microscopy.

1.2.1 The Importance of Stapes Motion

It is the footplate's direct attachment to the oval window that has made the stapes a focus of research into the mechanics of hearing, in that stapes motion is a measure of the output of the middle ear. Because of the dimensions of the inner ear–specifically that its dimensions are small in comparison with the wavelengths of audible sound–the inner ear can be modeled as an acoustic tube, with the oval window on one end and the round window, which serves as a pressure release, on the other. Furthermore, since measurements have been made of the acoustic impedance of the cochlea, stapes motion can completely characterize the input to the inner ear.

Not merely the magnitude of stapes motion, but the mode of those motions, as well, is crucial to a characterization of inner ear input. The stapes volume velocity[2] is the key measurement of inner ear input. In the simplest case, stapes motion would be entirely translational and along a vector perpendicular to the oval window. In that case, the volume velocity would be simply calculable as the product of velocity of the motions and the area of the stapedial footplate. However, with the introduction of some rocking component to the stapes motion, the relationship between motion and volume velocity becomes far more complex.

Because of the strong link between stapedial motion and hearing, a clear understanding of how the stapes moves in normal ears could prove important to clinicians. Conduc-

2. Volume velocity is an acoustic measure of flow. Beranek (1954) defines instantaneous volume velocity as the rate of flow of a medium perpendicularly through a specified area.

tive hearing loss–a disconnection of the bones of the middle ear–is the most commonly treated ear pathology. The current treatment is to reconstruct the middle ear such that the stapes moves in a piston-like fashion, but it is unclear whether the normal stapes moves in this fashion. A reliable model of stapes motion could either lead clinicians to more effective treatment of middle-ear trauma or assure them that current methods are adequate.

1.2.2 Stroboscopic Microscopy

Two of the major contributors to theories on stapes motion used forms of stroboscopic light microscopy, but came to very different conclusions. Georg von Békésy used mechanical arguments and human cadaver observations to come to the conclusion that there are two primary modes to stapes motion.[3] For sound pressure levels (SPLs) below the threshold of hearing, the stapes pivoted about the posterior tip of the footplate. For sound pressures above that threshold, the stapes rotated about an axis connecting the posterior and anterior tips of the footplate. Figure 1.3 illustrates these modes.

A few years later, Guinan and Peake at the Massachusetts Institute of Technology (MIT) and the Massachusetts Eye and Ear Infirmary (MEEI) challenged von Békésy's results with their own experiments on anesthetized cats. The results from Guinan and Peake are significant, because their measurements were made on live animals, as opposed to cadavers, but there are essential differences between human and feline ears. The feline ear is smaller than the human ear, and they differ in structure. The linear dimensions of the ossicles in the cat are about 60% of those of humans and the feline tympanic membrane and stapedial footplate have about 1/3 of the area of their human counterparts. As other animals with smaller ears, cats can hear sounds at higher frequencies than can humans, but cats also hear low frequencies as well as humans. Many previous experiments had been

3. Von Békésy (1960), p. 113.

performed on human cadavers, and there remains a question as to whether a live cat ear or a dead human ear better mimics a live human ear.

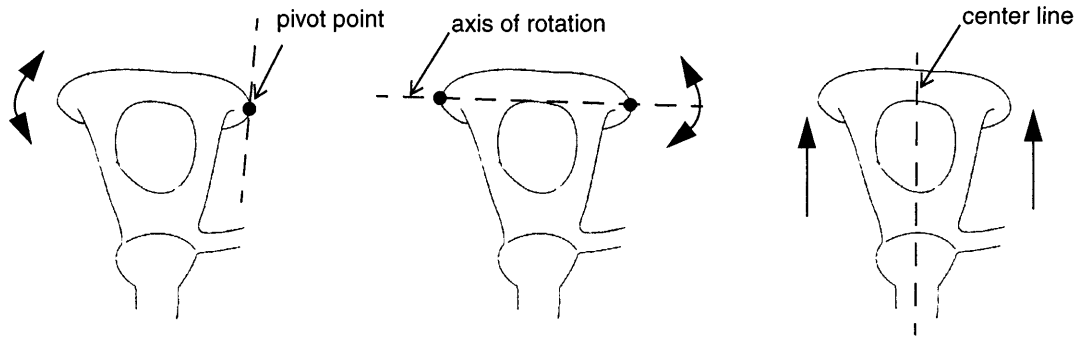

Figure 1.3: Three suggested modes of motion for the human stapes. Left was suggested by von Békésy for SPLs below the threshold of hearing. Center was suggested by the same for SPLs above that threshold. Right was suggested by Guinan and Peake.

Guinan and Peake observed microscopic motions of silver particles attached to the stapes while stimulating with sound and stroboscopically illuminating the middle ear. Motions were quantified by use of a microscope eyepiece micrometer.

Guinan and Peake found that for frequencies below 2 kHz, stapes displacement is a linear function of sound pressures up to 130 dB. Above 2 kHz, the upper bound for linearity was somewhat higher. An assessment of the degree of linearity is an important beginning step.

Beyond their assertion of linearity, Guinan and Peake found that the stapes moved as a rigid body. That is, they found no deformation of the crura. Their evidence came from a few test subjects in which they could actually view the footplate. This assumption, too, is crucial to any measurements made with the computer microvision system, because while motion estimates can usually only be made at the portion of the stapes near the head, the part of the stapes whose motion is directly linked to the cochlea, and hence hearing, is the footplate.

The crux of their results, however, was that within the range of sound pressure in which motion is linear, the stapes of anesthetized cats moves translationally along its center line–as a piston. Figure 1.4 summarizes the frequency response results from Guinan and Peake. For frequencies below 1 kHz, the near-zero phase and constant amplitude suggest that stapes motion is dominated by the compliance of the middle ear structures, including the tympanic membrane and the oval window membrane.

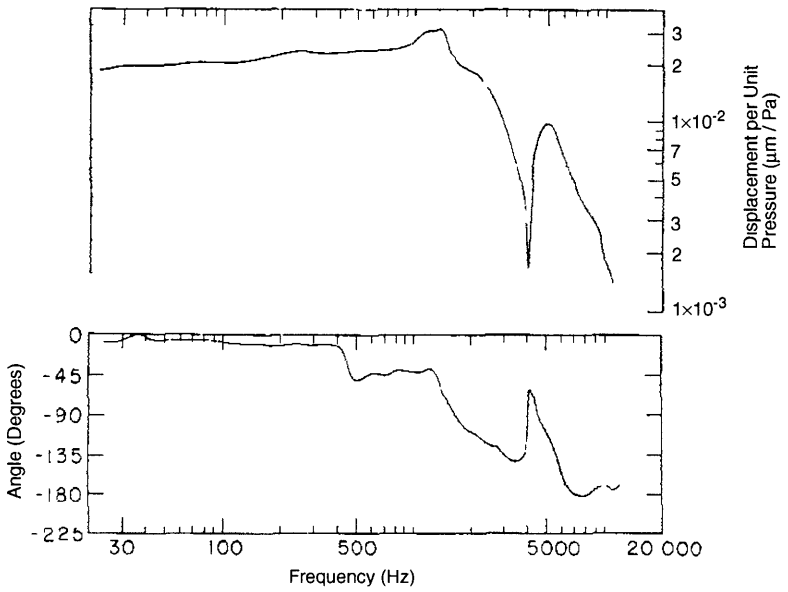

Figure 1.4: The frequency response of the feline ear: summary figure from Guinan and Peake (1967). Graph of the magnitude and angle of stapes displacement relative to the stimulus sound pressure at the tympanic membrane.

Further understanding of their results can be extrapolated from a simplified, lumped-parameter model of the system. Using an impedance analogy to electrical systems in which velocity is the across variable and force is the through variable, we can understand compliances as capacitances, masses as inductances, and dashpots as resistances. Viewing the system in terms of an electrical circuit, it appears as an RLC circuit, where the capacitance dominates the response for frequencies below resonance. Figure 1.5 illustrates a cir-

cuit that could provide insight for low-frequency responses up to approximately 4 kHz. In that range, the magnitude of the displacement (analogous to the charge stored in the capacitor) is a constant with respect to frequency, and stapes displacement and the sound pressure at the tympanic membrane (a scalar multiple of the current I_{tm}) are in phase. The resonant frequency is approximately 1.2 kHz. Above that frequency, the magnitude of the displacement falls off rapidly.

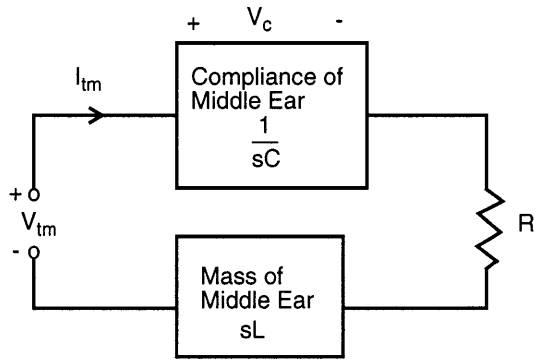

Figure 1.5: Block diagram of a lumped-parameter model derived from Guinan and Peake. Stapes displacement is analogous to the charge stored in the capacitor, which is also the derivative of the current I_{tm}. The velocity at the tympanic membrane V_{tm} is due to a transducer, which can be characterized as a velocity source.

A great disadvantage to the methods used by Guinan and Peake was that they had to use SPLs far above normal physiological levels in order to obtain visible stapes motion. In general, they used SPLs ranging from 100 to 150 dB to produce displacements that varied between 0.5 and 30 μm. Considering that 130 dB is the level at which permanent hearing damage begins to occur, that range is far from the physiologic norm. Their assumption was that as long as measurements are made at SPLs in the range where displacement is a linear function of SPL, those measurements are valid indications of the motion at lower SPLs, as well.

1.2.3 More Modern Methods.

Many of the modern measurement systems which have been used on the middle ear involve single-point measurements. Laser interferometry can measure motions with nanometer accuracy, but in only one direction. It is up to the experimenter to obtain measurements from various orientations in order to quantify three-dimensional motions. It is also generally necessary to place reflectors on the moving object. Other unidirectional motion measuring techniques include capacitive probe methods, which involve the measurement of an electrical signal obtained from the motion of a probe placed near the membrane, and the Mössbauer method, which quantifies motion by measuring the modulation of gamma radiation.

1.3 Use of Temporal Bones

All of my stapes motion measurements were performed on a human cadaver temporal bone preparation which was approximately one year old and which had been frozen and thawed numerous times. Questions regarding the use of such preparations to quantify the properties of the middle ear of live humans demand some consideration. Three key questions seem to arise: whether even fresh cadaver material behaves as the middle ear of live humans, whether freezing the tissue significantly alters its behavior, and whether an age of up to one year significantly degrades the preparation.

Because it remains impractical to measure stapes motion directly in live humans, there is no definitive way to establish the relationship between the action of the human middle ear before and after death. Until such measurements are possible, any descriptions of such a relationship will remain speculation based on related indicators in live humans or on data from fresh human cadavers or from animals other than humans. Von Békésy[4] suggests

from observations of tympanic membrane motion immediately after death that the decrease in magnitude of those motions due to the onset of *rigor mortis* is at most a factor of three. Guinan and Peake,[5] however, assert that the usefulness of human cadaver material is questionable.

Two more recent studies suggest that variations in ear motion due to death are no greater than the variations among test subjects. Goode et al.[6] measured the displacement of the umbo–the functional center of the tympanic membrane–with a laser doppler vibrometer. Their test subjects included six normal, live humans and 15 fresh human temporal bone preparations. They found that measurements in both types of test subjects had approximately the same mean and variance. Umbo motion in fresh cadavers appears to be indistinguishable from the same in live subjects.

The other study came to similar conclusions through measurements of sound pressure at the tympanic membrane. Rosowski et al.[7] measured the acoustic impedance of the middle ear by use of a sound source and microphone coupled to the external auditory canal. The sound pressure at the tympanic membrane when the system was driven by a sound source of known characteristic yielded a measurement of middle ear impedance. Their test subjects included live humans, human temporal bones, and guinea pigs. Similar to the results from Goode et al., they found that there was little difference between the acoustic impedance of live and cadaver middle ears, especially in the frequency range from 200 Hz to 2 kHz. Using the guinea pigs, Rosowski et al. measured the time course of the middle ear impedance for sixteen hours after death, at which point the temporal bone was

4. Von Békésy (1960), p. 112.
5. Guinan and Peake (1967), p. 1237.
6. Goode et al. (1993).
7. Rosowski et al. (1990).

removed and a final impedance measurement made. For frequencies below 1 kHz, the changes appeared negligible.

The results from Rosowski et al. have implications not only for the first question, but for the other two, as well: whether freezing and thawing and whether age have a significant effect on the properties of a temporal bone preparation. Their results regarding fresh versus thawed preparations is inconclusive. Some of their preparations had considerably different impedances after being frozen and thawed once, while others appeared unaffected. They found, however, that once a bone had been frozen, there was little change in its properties after repeated freezing and thawing.

The crux of the results from Rosowski et al.–part of which are directly supported by Goode et al.–was that human temporal bones are a reliable test subject, so long as care is taken to keep them moist. That assertion of reliability gives some justification for the use of human temporal bones as subjects on which to measure stapes motion. One can imagine that if the overall response of the middle ear is stable after death, it is not entirely unreasonable to assume that stapes response will remain stable, as well.

1.4 Computer Microvision Measurements

Recently, at MIT, a new measurement system dubbed *computer microvision* has been developed. This system has been demonstrated to measure three-dimensional, rigid-body translation to a resolution on the order of nanometers. Such accuracy is quite a feat considering that the wavelength of the light used by the system is approximately 525 nm. The computer-controlled system uses a strobing light source, a microscope, and a digital camera to create time sequences of magnified light photographs. A computer algorithm then estimates sub-pixel motions by a gradient technique, which uses information from the

change in brightness of the pixels in an individual image and their spatial relation to each other to determine two-dimensional motion in the plane of the stage of the microscope. The algorithms are largely borrowed from the field of computer vision. The system uses similar means to calculate the vertical, out-of-plane motion, but uses added information from how the brightness of the pixels changes between images taken at different heights when the stage is moved in the vertical direction with a computer-controlled stepper motor.

The primary motivation behind the development of computer microvision was for use on biological structures, but the system has been used on microelectromechanical systems (MEMS), as well as two inner-ear structures: the tectorial membrane of the mouse and hair bundles in the cochlea of the alligator lizard. Some preliminary human middle-ear measurements have also been made using the system. As a computer microvision test target, the human stapes is perhaps most similar to MEMS, because both are opaque to the wavelengths of light used by the system. The tectorial membrane and the cochlea are nearly transparent, so experimenters can use transmitted light to illuminate those targets.

The purpose of this new work is to use computer-based advances in the measurement of three-dimensional microscopic motions to address the issue of how the human stapes moves with near normal sound levels. Computer microvision measurements have something new to contribute to questions about stapedial motion, because of the accuracy with which the system can detect small amplitudes of motion simultaneously in three dimensions. Due to that accuracy, I can make measurements at physiologic SPLs and attempt to characterize stapedial motion, quantifying to what degree computer microvision measurements corroborate the various motion theories.

Chapter 2

Methods

My methods have three logical divisions: the image acquisition and processing method common among computer microvision measurements, the sound stimulus, and the human temporal bone preparation.

2.1 Computer Microvision

Computer microvision measurements involve two steps: image acquisition and image processing. Through a microscope, a digital camera takes stop-action images of a target stimulated by an electrical signal from the computer. The stimulus signal, which in the case of my measurements drives a sound source, is synchronized to a strobing LED. After images have been acquired at the desired times and planes of focus, computer algorithms estimate the rigid-body translation of structures in the images chosen by the experimenter. While it is the processing that gives the motion measurement results, accurate results depend on images of sufficient quality.

2.1.1 Image Acquisition

The microscope set-up includes a Zeiss Axioplan microscope mounted atop a pneumatically suspended, vibration-isolated table. A Photometrics CE 200A charge-coupled device (CCD) camera is mounted on the microscope, so that pictures can be taken of what would otherwise be seen through the eyepiece. The targets are epi-illuminated with a green LED[1], which is sent through a low-angle deflector to diffuse the light's fixed pattern.

1. Wavelength of light 525 nm. Output power 2 mW.

While a lower-power (5×) objective was used to survey the specimen, images were acquired using 20× magnification.[2]

The camera is dubbed a charge-coupled device due to the manner in which it reads out the charge wells that correspond to individual pixels in the images. Such a device can be described as sampling the light intensity at discrete points along the plane of focus. The charge wells form a sort of bucket brigade, each dumping its charge into the next well, while the wells on the end are quantized.

To compute stimulus-induced motion, information is gathered at different times during the stimiulus cycle. Using the `ledvol`[3] program, images are taken at 8 equally spaced points during a period of the input voltage waveform. With the camera shutter open, the LED pulses repeatedly at one phase of the waveform. The pulse width of the LED can be as short as 1 μs.[4] When enough light[5] at that phase has been collected to expose the image, the intensities are quantized and stored, and the LED pulses at the next chosen phase of the waveform. Processing of these time-sampled images will yield two-dimensional motion estimates in the plane of the microscope stage.

Motion estimates in the vertical[6] or out-of-plane direction are derived from a set of eight time-sampled images at each of several evenly spaced vertical sections. The stage of the microscope is controlled by a stepper motor, allowing the stage to be moved up and down in increments of 1/11 μm. After the `ledvol` program has acquired all eight images at a given level, the stage is moved downward, so that the plane of focus moves up the tar-

2. Objective: Zeiss LD-Epiplan, #442840, 0.4 NA, 9.8 mm working distance.
3. See appendix A.
4. Davis (1997), p. 127
5. The default value for total LED duration (some integer multiple of the single LED pulse duration) is 62 ms, but it can be adjusted.
6. Permit me to define vertical as perpendicular to the microscope stage. Horizontal refers to the plane of the stage. Further, I define the z-direction as the vertical, the x-direction as toward the right of the observer, and the y-direction as away from the observer. This sense is preserved in subsequent images.

get, and another set of images is taken. The complete set of images–8 per focal plane for each of 16 to 40 focal planes–is referred to as a *volume*.

2.1.2 Image Processing

Image processing begins with the definition of a small region of interest (ROI), i.e., a region assumed to move as a rigid body. When the experimental target is silicon, as with MEMS, the rigid body approximation is an accurate one. However, when the target is human tissue or even a plastic membrane, that approximation is no longer so obviously valid, so care has to be taken to choose a reasonable region.

In addition to the definition of regions of interest, the acquisition of two further images is necessary before processing can begin. The first image is a *dark picture* taken with the camera shutter closed, which provides a measure of internal artifacts due to the camera itself. The second image–the *background* or *bright field picture*–provides a measure of the artifacts due to the optics or the pattern of the light source. This picture is taken of a silicon mirror and is averaged several times to decrease the effect of the stochastic nature of image acquisition. The dark and background images are used in a two-point correction technique that serves to reduce fixed pattern noise. For each pixel contained in a region of interest, the corrected brightness value is obtained by dividing the raw value by the background value, after first subtracting each by the corresponding dark value. That is,

$$\text{Corrected} = \frac{\text{Raw} - \text{Dark}}{\text{Background} - \text{Dark}}. \tag{2.1}$$

This two-point correction method has been demonstrated to reduce the fixed-pattern noise by a factor of three, while increasing the shot noise by an insignificant amount.[7]

7. Davis and Freeman (1997).

After the region of interest has been chosen, the images and accompanying information are fed to the processor, which crops the images according to the region of interest and then feeds those images to the computer microvision algorithms, resulting in three-dimensional displacement values for each of the eight sampled phases of the stimulus waveform, as well as fast Fourier transforms (FFTs) of those displacements.[8]

The computer microvision algorithms inspect the intensity gradients of the images and use that information to estimate subpixel, two-dimensional motions. Motion estimates in the vertical direction are obtained by a gradient method, as well. The corresponding images at the same time and different vertical level serve as samples as did the pixels of the individual images in the two-dimensional case.

2.2 Sound Stimulus

A stimulus sound pressure was applied to the subject by use of a transducer controlled by the computer.

2.2.1 The Electrical Set-up.

The strobing light source is synchronized to the variable-frequency output of a digital-analog converter (DAC). The DAC output is run through a low-pass filter[9], which serves as a reconstruction filter. The signal is run through a Crown D-75 power amplifier, an oscilloscope or signal analyzer, and then to the sound source. The sound source is a transducer that has an internal, active microphone. The microphone has a short probe tube to

8. `2ptnormcrpr3dflow`. See Appendix A.
9. The reconstruction filter is an 11-pole, elliptical low-pass filter, with a 3kΩ in/out impedance. Pass band: 3dB 0-20 kHz. Stop Band: -80dB @ 25kHz.

minimize tube-related delays. Figure 2.1 is a block diagram of this sound source apparatus.

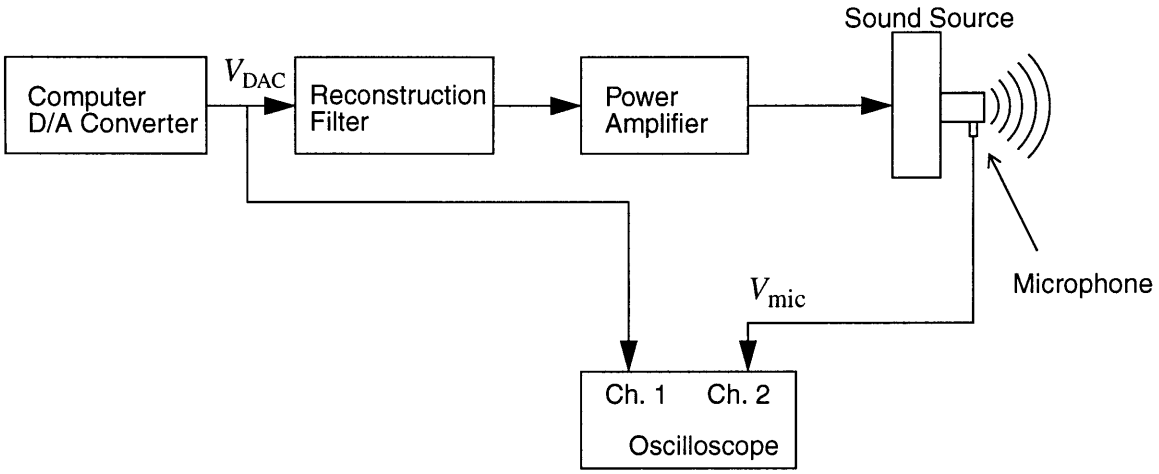

Figure 2.1: Acoustic Apparatus

2.2.2 Measurement of Stimulus Sound Pressure

In order to estimate the middle-ear transfer function, the stapes motion measurements must be normalized to the input to the middle ear, i.e. the sound pressure at the tympanic membrane. This sound pressure can be determined from measurements of microphone voltage, the measured frequency response of the transducer with respect to its input voltage signal, and the frequency response of the entire system with respect to the signal output of the DAC.

The microphone was calibrated against a reference microphone using a broad-band chirp (signal frequency varies linearly with time) input of known SPL, yielding a frequency response of sound pressure with respect to microphone voltage. It was calibrated with a microphone placed approximately where the tympanic membrane would be. Similarly, the magnitude and angle of the microphone output voltage with respect to the DAC output voltage was determined for key frequencies and amplitudes using a Hewlett-Pack-

ard 3562A dynamic signal analyzer. When I make motion measurements, I measure target displacement at a known DAC output V_{DAC} (H_1 below); I then divide by the transfer function of microphone voltage V_{mic} with respect to V_{DAC} (H_3 below) and divide by the transfer function of sound pressure with respect to microphone voltage (H_2 below) to obtain displacement with respect to sound pressure. That is,

$$\text{given } H_1 = \frac{\text{displacement}}{V_{DAC}} \qquad H_2 = \frac{\text{SPL}}{V_{mic}} \qquad H_3 = \frac{V_{mic}}{V_{DAC}},$$

$$\frac{\text{displacement}}{\text{SPL}} = \frac{H_1}{H_2 H_3}. \tag{2.2}$$

It should be noted that H_3–the relationship between the output of the microphone and the DAC input–is dependent upon the system to which the sound source is coupled.

The basic assumption in this calculation is that sound pressure is linearly related to input voltage. In reality, I have H_1 and H_3 only as voltage or displacement values for a given DAC amplitude of V_{DAC}, but I assume that, within the range of values I use, the amplitudes are linearly related.

2.3 Human Temporal Bone Preparation

Experimentation on human cadaver material began with a frozen temporal bone preparation obtained from the MEEI and prepared by John Rosowski.[10]

A clear plexiglass platform is mounted with screws to a maneuverable stage. An aluminum petry dish is mounted with plasticene to the plexiglass, and the temporal bone is fixed in place with clay. The transducer is mounted to the stage and is interfaced to the bone via clay and a ring cemented to the bone. Plastic tubing is used to drip saline over the

10. For details regarding preparations of this type, refer to Rosowski et al. (1990).

top of the bone to keep it moist, while another tube attached to a peristaltic pump suctions excess fluid from the petry dish. Figure 2.2 is a sketch of this set-up.

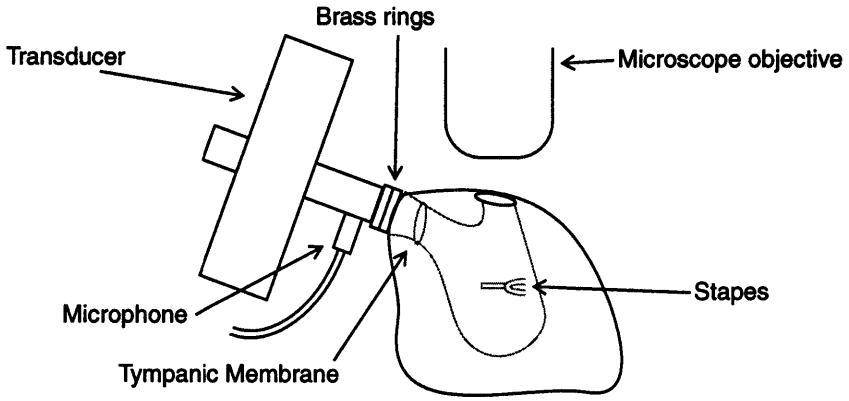

Figure 2.2: Temporal Bone Set-up

The temporal bone has been cleaned so that it will fit in the small region between the microscope objective and the stage. A hole has been drilled through the top of the bone which allows the microscope a direct view of the head of the stapes. Holes are drilled on either side of the preparation to allow the experimenter to view the orientation of the ossicles.

An issue which arises in the orientation of the temporal bone is the short working distance of the microscope objectives. I use a 5× objective to identify major structures in the preparation and use a 20× objective to make the computer microvision measurements. As a means of identifying the relationship between pictures taken with the two objectives, silver particles were strewn on the stapes. The working distance for the two objectives is approximately 1cm, and the stapes is typically at a depth of nearly 1 cm below the upper edge of the temporal bone, which gives little room for variation in the position of the preparation.

Chapter 3

Method Testing and Technical Considerations

Various tests were performed before making computer microvision measurements of stapedial motion. These tests served to familiarize me with the requirements for accurate results and their interpretation, as well as to adjust current computer microvision technique to this new application.

3.1 Tests of the Technique

3.1.1 The Plastic Diaphragm

For a preliminary test target, I measured the sound-induced motions of a thin, plastic diaphragm. The plastic membrane had the advantages of being inexpensive and having predictable and verifiable motion characteristics. It was stretched across a short piece of brass tubing of approximate diameter 0.5 cm, and held in place by another piece of brass tubing which fit snugly over the first. I performed a frequency response test on the membrane and compared it against measurements made at MEEI with a laser doppler vibrometer.

3.1.2 Diaphragm Frequency Response

I swept frequency from 20 to 10240 Hz, keeping the DAC amplitude constant at 50 mV. At 50 mV, the actual SPL varies from 105 to 117 dB SPL. Figure 3.1 shows the magnitude and phase for all three directions of diaphragm motion versus the stimulus frequency. The motions are normalized to the sound pressure produced by the stimulus at the

corresponding frequency. That the magnitudes in the out-of-plane direction (or $\hat{t}_z$, represented by solid lines) are consistently higher than those in the other two directions suggests that diaphragm motion is predominantly in the direction perpendicular to its surface. The near-zero phase component of the out-of-plane motions suggests that for frequencies below 2 kHz, the diaphragm motions are in phase with the sound pressures generated by the stimulus.

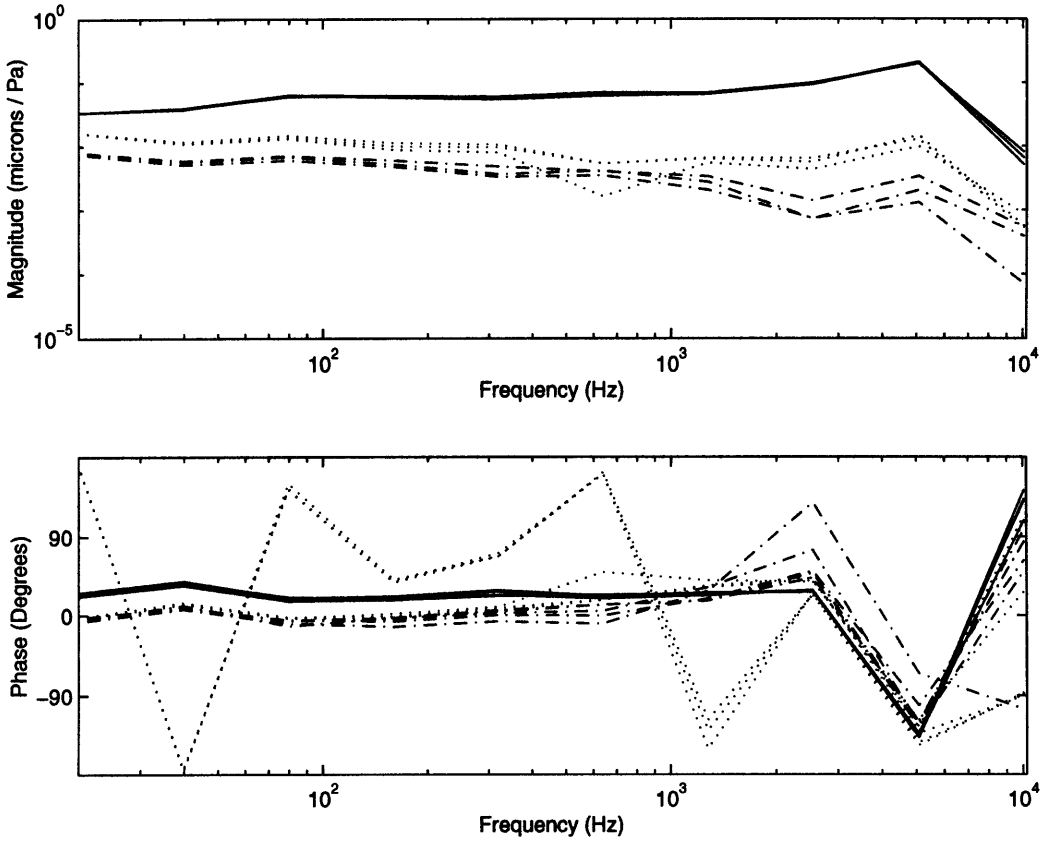

Figure 3.1: Magnitude and phase components of plastic diaphragm motion in all three directions. Solid lines are vertical or z-directed motions. Dotted lines are x-directed (toward the right) motions. Dashed lines are y-directed (away from observer) motions. Motions are normalized to the stimulus sound pressure.

I compared these results with measurements made at the Eaton-Peabody Laboratory of the MEEI using a laser doppler vibrometer, which measures unidirectional velocity. Figure 3.2 shows the z-directed results from figure 3.1 plotted on the same axes as the dis-

placement estimates obtained with laser measurements. Displacements were calculated from the laser-doppler system's velocity measurements by steady-state integration.

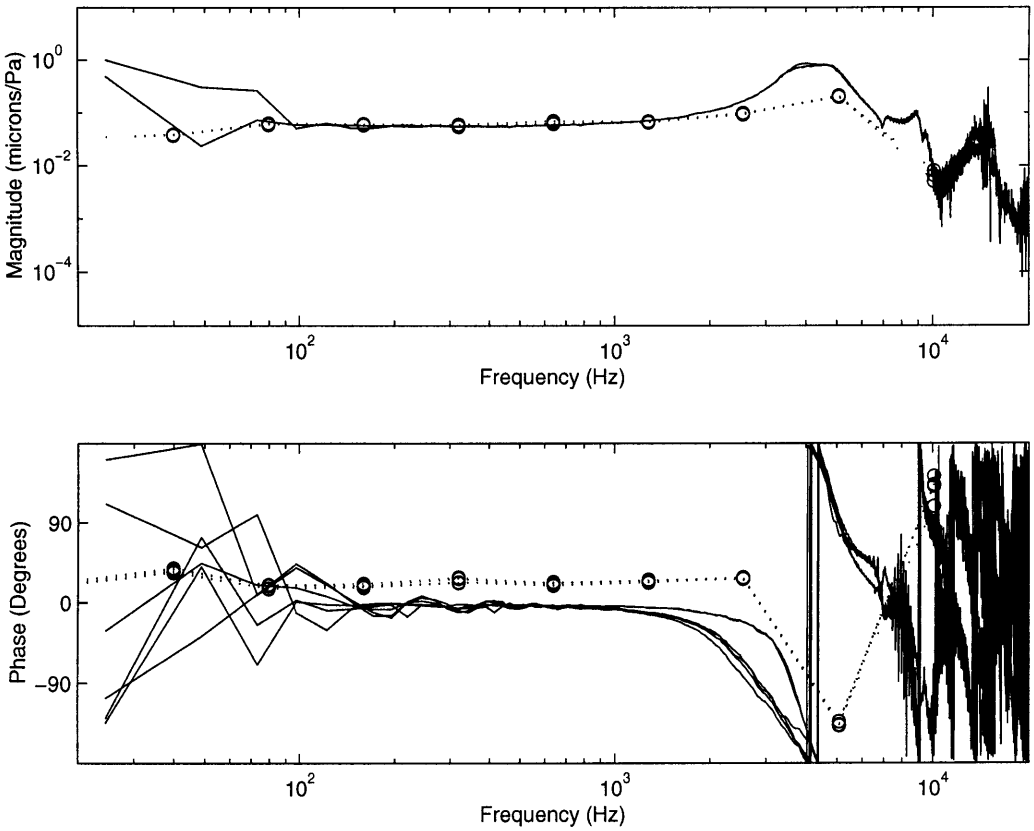

Figure 3.2: Frequency response of the plastic diaphragm. Solid lines are results from laser-doppler measurements. Circles connected by dotted lines are data points obtained using computer microvision.

For frequencies below approximately 100 Hz and above approximately 10 kHz, the laser measurements become noisy. In the range where the magnitudes of the laser response are not noisy, the greatest discrepancy between the laser and computer microvision measurements occurs at 6 kHz, where the laser-obtained magnitude is about three times the magnitude reported by computer microvision.

The frequency response of the diaphragm displacement bears some resemblance to the stapes results from Guinan and Peake, confirming that it was a good choice as a test target. The peak in the magnitude plot and the sudden change in the phase plot suggest that the system has a resonant frequency somewhere near 4.5 kHz. For frequencies below reso-

nance, the phase is constant near zero and the magnitude is also constant. Using the same lumped-parameter analysis as in the stapes results, the diaphragm motions are dominated by compliance for frequencies below resonance. Above resonance, the behavior is erratic and difficult to characterize.

3.2 Directional Analysis

The computer programs which implement computer microvision algorithms yield results in terms of the Cartesian coordinate system of the images themselves, where $\hat{\imath}_x$ is to the right, $\hat{\imath}_y$ is up the image or away from the observer, and $\hat{\imath}_z$ is the direction perpendicular to the image. However, this set of axes is not always the most useful frame of reference. In the case of temporal bone preparations, it is often not possible to orient the target in such a manner that the important features in the image move primarily along any one of the three axes. In answer to this concern, I reorient my results along an empirically suggested set of axes.

The output of the computer program that performs motion estimation[1] is the least-squares estimate of the displacement in three dimensions at each of eight time points and the fast Fourier transform of those displacements. The program computes an eight-point FFT, which consists of magnitude and phase information for four positive frequencies and their negatives. Taking advantage of the symmetry property for the transform of real-valued signals, the program only reports the magnitude and phase for postive frequencies. Essentially, this FFT output decomposes the displacement into the sum of four scaled, shifted sinusoids: one at the fundamental–the frequency of the stimulus–and one at each of the next three harmonics–2, 3, and 4 times the stimulus frequency. In the accurate mea-

1. `2ptnormcrpr3dflow`. See Appendix A.

surement of an ideal linear system, only the fundamental would have a nonzero magnitude.

Because I expect the displacement of the human stapes with respect to the sound pressure at the tympanic membrane to be a linear system, I assume that the magnitudes at the higher-order harmonics are small compared to that at the fundamental frequency. Therefore, a natural choice for a coordinate system would seem to be that defined by the three-dimensional, sinusoidal motion at the fundamental frequency. Single-frequency, sinusoidal motion in three dimensions invariably traces out some ellipse[2]. The Cartesian coordinate system I define is one in which $\hat{\imath}_l$ is the lesser direction of motion (along the minor axis of the ellipse), $\hat{\imath}_m$ is the major direction of motion (along the major axis of the ellipse) , and $\hat{\imath}_n$ is the null direction (perpendicular to the plane of the ellipse). At the fundamental frequency, the magnitude in $\hat{\imath}_n$ must be zero.

A MATLAB script[3] implements the change of coordinates as follows.

As the FFT decomposition suggests, position evolves with time as the sum of four sinusoids of different frequency in each of the three coordinate directions. That is,

$$\text{position } \boldsymbol{r}(t) = \sum_{k=1}^{4} \boldsymbol{r}_k(t), \text{ where}$$

$$\boldsymbol{r}_k(t) = \hat{\imath}_x|x_k|\cos(kt + \angle x_k) + \hat{\imath}_y|y_k|\cos(kt + \angle y_k) + \hat{\imath}_z|z_k|\cos(kt + \angle z_k), \tag{3.1}$$

and where the normalized time t is the product of the fundamental frequency and time in seconds. Each $\boldsymbol{r}_k(t)$ corresponds to the elliptical motion at k times the fundamental frequency. If the target responds linearly, the magnitude of motion at the fundamental frequency will be much greater than that of the other three harmonics. Ignoring the effects of noise, the magnitudes at higher-order harmonics, then, are an indication of the amount of nonlinearity in the system.

---

2. A straight line–also a possibility–can be thought of as an ellipse of zero width.
3. See Appendix B.

Each vector $\boldsymbol{r}_k(t)$ over time traces out some ellipse in three-dimensional space. In the expectation that the systems I measure will be largely linear, I want to read the FFT data in terms of a coordinate system in which the l-m plane is the plane of the ellipse traced out by fundamental frequency motion $\boldsymbol{r}_1(t)$. That is, I want to rewrite the position expression (3.1) as

$$\boldsymbol{r}_k(t) = \hat{\imath}_l|l_k|\cos(kt + \angle l_k) + \hat{\imath}_m|m_k|\cos(kt + \angle m_k) + \hat{\imath}_n|n_k|\cos(kt + \angle n_k),$$

$$\text{where } |n_1| = 0, \text{ and } |m_1| \text{ is maximized.} \tag{3.2}$$

In order to identify the major direction of motion, $\hat{\imath}_m$, I need only concern myself with $\boldsymbol{r}_1(t)$. The major direction of motion is where the $\boldsymbol{r}_1(t)$ vector points at the normalized time when the distance from the origin is at a maximum. That is,

$$t_{\max} = \arg\max_{t} \left(d(t) = \sqrt{(|x_1|\cos(t + \angle x_1))^2 + (|y_1|\cos(t + \angle y_1))^2 + (|z_1|\cos(t + \angle z_1))^2}\right). \tag{3.3}$$

Because the distance from the origin is a nonnegative quantity, it is equivalent to maximize the square of the distance $d^2(t)$, setting its derivative equal to zero. Since the path of $\boldsymbol{r}_1(t)$ is some ellipse, there are two times per cycle at which the distance is a maximum and two times per cycle at which the distance is a minimum. The roots of $\frac{d}{dt}(d^2(t))$ satisfy the equation

$$t_{\max}, t_{\min} = \angle x_1 - \frac{1}{2}\operatorname{atan}\left(\frac{|y_1|^2\sin 2(\angle y_1 - \angle x_1) + |z_1|^2\sin 2(\angle z_1 - \angle x_1)}{|x_1|^2 + |y_1|^2\cos 2(\angle y_1 - \angle x_1) + |z_1|^2\cos 2(\angle z_1 - \angle x_1)}\right). \tag{3.4}$$

There are four solutions to the equation in one revolution of the unit circle. I can eliminate one each of the maxima and minima by using a four-quadrant arctangent function[4], but in order to distinguish between $t_{\max}$ and $t_{\min}$, I have to evaluate $d(t)$ to see at which time the position is further from the origin. Having determined $t_{\max}$ and $t_{\min}$, I know that

4. In MATLAB, `atan2` uses sign data from the numerator and denominator to determine in which of the four quadrants the angle belongs.

$$\hat{\imath}_m = \frac{\boldsymbol{r}_1(t_{\max})}{d(t_{\max})}, \tag{3.5}$$

$$\hat{\imath}_l = \frac{\boldsymbol{r}_1(t_{\min})}{d(t_{\min})}, \text{ and} \tag{3.6}$$

$$\hat{\imath}_n = \hat{\imath}_l \times \hat{\imath}_m. \tag{3.7}$$

The directions $\hat{\imath}_l, \hat{\imath}_m, \hat{\imath}_n$ are now expressed as linear combinations of the directions $\hat{\imath}_x, \hat{\imath}_y, \hat{\imath}_z$, and I define the matrix A as one satisfying the equation

$$A\begin{bmatrix}\hat{\imath}_x\\ \hat{\imath}_y\\ \hat{\imath}_z\end{bmatrix} = \begin{bmatrix}\hat{\imath}_l\\ \hat{\imath}_m\\ \hat{\imath}_n\end{bmatrix}. \tag{3.8}$$

The matrix A should be invertible, unless the motion is along a straight line in the $\hat{\imath}_m$ direction, in which case no determinate $\hat{\imath}_l$ or $\hat{\imath}_n$ exists. If A is invertible, then I can obtain

$$A^{-1}\begin{bmatrix}\hat{\imath}_l\\ \hat{\imath}_m\\ \hat{\imath}_n\end{bmatrix} = \begin{bmatrix}\hat{\imath}_x\\ \hat{\imath}_y\\ \hat{\imath}_z\end{bmatrix}. \tag{3.9}$$

With $\hat{\imath}_x, \hat{\imath}_y, \hat{\imath}_z$ expressed as linear combinations of $\hat{\imath}_l, \hat{\imath}_m, \hat{\imath}_n$, I can substitute those linear combinations into the equation (3.1) for $\boldsymbol{r}_k(t)$. After some algebra, I obtain

$$\boldsymbol{r}_k(t) = (A^{-1})^{\mathrm{T}}\left(\begin{bmatrix}|x_k|\\ |y_k|\cos(\angle y_k - \angle x_k)\\ |z_k|\cos(\angle z_k - \angle x_k)\end{bmatrix}\cos t - \begin{bmatrix}0\\ |y_k|\cos(\angle y_k - \angle x_k)\\ |z_k|\cos(\angle z_k - \angle x_k)\end{bmatrix}\sin t\right)\begin{bmatrix}\hat{\imath}_l\\ \hat{\imath}_m\\ \hat{\imath}_n\end{bmatrix}. \tag{3.10}$$

The desired expression for $\boldsymbol{r}_k(t)$ (as in equation 3.2) is derived from equation 3.10 by use of the identity:

$$a\cos t + b\sin t = \sqrt{a^2+b^2}\cos\left(t - \operatorname{atan}\left(\frac{b}{a}\right)\right). \tag{3.11}$$

In order to interpret the new coordinate directions, I need to express the new coordinate system as some rotation of the old system. If ϕ and θ are the angles of a spherical

coordinate system based on $\hat{\imath}_x, \hat{\imath}_y, \hat{\imath}_z$, such that $\phi = \text{atan}\left(\frac{y}{x}\right)$ and $\theta = \text{atan}\left(\frac{\sqrt{x^2 + y^2}}{z}\right)$, then $\hat{\imath}_m$ is along the ray where

$$\phi = \text{atan}\left(\frac{A_{2,2}}{A_{2,1}}\right) \text{ and } \theta = \text{atan}\left(\frac{\sqrt{(A_{2,2})^2 + (A_{2,1})^2}}{A_{2,3}}\right). \tag{3.12}$$

As indicated in the definition of the matrix A, $A_{2,1}$, $A_{2,2}$ and $A_{2,3}$ are the x, y, and z components, respectively, of the $\hat{\imath}_m$ vector.

3.3 Image Quality

Accurate computer microvision measurements require volumes of images that are of sufficient quality. Many factors contribute to the quality of an individual image, including mean pixel brightness, total magnification, microscope adjustment, and the characteristics of the microscope objective[5]. Two further factors contribute to the quality of volumes: the vertical (z) distance between planes of focus and the total vertical range the planes of focus collectively cover. That is, if a particular volume consists of 8 pictures taken at each of 16 planes of focus 1 μm apart from each other, then the vertical distance between focal planes is 1 μm and the total vertical range–or *depth range*–is 15 μm.

Care must be taken to adjust the microscope properly in order to avoid tube reflections. When they occur, light is wasted on these internal reflections, thus less light is available to illuminate the target.

Further, images should be taken in the approximate middle of the dynamic range of pixel intensity. The camera has a 12-bit quantizer, so the mid-range of the intensity is pixel values around 2000. The reasoning behind this precaution is to reduce the effect of quanti-

5. The essential characteristics of a microscope objective are its gain and its *numerical aperture*–a gauge of the objective's blurring effect.

zation. Photons strike the charge wells as a Poisson process[6]. The amount the quantized value differs from the analog value is a larger percentage of that analog value when intensity is low. It is also essential to avoid saturation, because computer microvision algorithms cannot accurately track saturated pixels. This result is understandable, since saturated pixels report no positive changes in intensity and may underrepresent negative changes.

An interpretation of image acquisition in terms of a sampling process aids in the explanation of some of the other factors contributing to image quality.

The CCD camera's acquisition of volumes of images can be understood as a sampling process–a three-dimensional analog of the sampling concept for time waveforms. In the idealized sampling of a time waveform, the value of some continuous-time waveform is recorded at evenly spaced, discrete points to create some discrete-time waveform. The discrete-time waveform is a faithful representation of its continuous-time counterpart to some frequency determined solely by the spacing of the samples. That is, the continuous-time waveform can be completely recovered from the discrete samples only if the continuous-time signal has no content of frequency greater than $\frac{1}{2T}$, where T is the time between samples.

The acquisition of a single image can be viewed as a two-dimensional analog of the sampling of a time waveform. The microscope casts light on the camera, and the variations in the intensity of this light are continuous along two spatial axes: x and y. In producing an image from this light, the camera discretizes a spatially continuous signal. Whether the discrete signal is a faithful representation of its continuous counterpart is a valid concept in this two-dimensional case, as well. Assuming that all characteristics of the micrscope objective remain unchanged, the total magnification controls the sample spacing.

6. Discrete-time random process, where the mean and variance are equal.

Under higher magnification, the pixels of the resultant image are effectively closer spaced samples of the same light signal. As in the time analog, closer sample spacing results in a faithful representation of higher frequencies, though in the case of images, frequency is not the rate with which signal values change in time, but in two-dimensional space.

This concept can be extended to include an understanding of the acquisition of a volume of images as a sampling process. In the case of a volume, individual images are samples of a light signal that varies continuously in three spatial dimensions[7]. The distance between samples, then, is the vertical distance between images in a volume–or *step size*. If the samples are spaced more closely together, then higher spatial frequencies can be resolved in the vertical direction.

With an understanding of volume acquisition as a sampling process, it becomes clear that care must be taken to avoid aliasing–the inaccurate representation of high frequency components. Specifically, *spatial aliasing* can be avoided by taking individual pictures at a sufficiently high magnification and by choosing a sufficiently small vertical step size for volumes.

3.3.1 Spatial Aliasing in Individual Images.

Information losses due to spatial aliasing in individual images could conceivably affect the accuracy of computer microvision motion estimates. To prevent spatial aliasing given a particular objective, I need only to adjust the total magnification of the microscope. However, this adjustment must be done in such a way that the change in magnification does not introduce any changes to the light signal other than magnification. Such a change in magnification is possible on the Zeiss Axioplan microscope; an instrument called the *optivar* is

7. The characteristics of this three-dimensional light signal are due to the target and the way in which the microscope blurs the image–the *point spread function* of the microscope. See Kaiser (1997).

capable of increasing the total magnification up to a factor of 2.5. While an increase in magnification may be necessary to avoid spatial aliasing, the disadvantage to such an increase is that less light will be available for the image–a condition that could lead to longer camera exposure times.

To determine experimentally the minimum total magnification required to prevent aliasing using the 20× objective, I took pictures of a MEMS. The MEMS was chosen, because an image of it will contain significant levels at high spatial frequencies. That is, because the object has sharply contrasted edges, images of it will have pixel intensity values that change rapidly along spatial axes. The images were taken with each of four settings of the microscope optivar, which increases the overall magnification of the images by a factor of 1, 1.6, 2.0, or 2.5. I then processed the images with a two-dimensional FFT algorithm[8] and compared the FFT magnitude plots of the various images, searching for signs of aliasing. Inspection of the FFT images suggests that the 1.0× optivar setting should suffice to avoid spatial aliasing.

3.3.2 Sampling along the Vertical Axis

Two factors come into play in deciding at which planes of focus I should acquire images. First, much of the important information regarding movement of the subject in the vertical direction is actually in the planes of focus as much as 15 μm above the subject. This phenomenon is due to the point spread function of the microscope[9]. The depth range needed for any particular experiment depends upon the magnitude of the motions of the subject and the characteristics of the objective. Second, it is crucial that I not undersample

8. `fft`. See appendix A.
9. See Kaiser (1997).

along the vertical axis by acquiring images at too great a vertical separation from each other.

I confirmed the first assertion by examining a volume of images of the human temporal bone preparation with no stimulus. The volume consists of one picture at each of 200 vertical levels, each 5/11 μm from the previous level. I then took the difference[10] of each pair of consecutive images and noted that at 10 μm from the plane of focus, the difference in intensity between consecutive pictures was at a maximum. Because computer microvision uses the gradient of intensity as the criterion for measuring motion, the area of highest gradient is where much of the motion information is located. Figure 3.3 shows the results of that difference test. The peak around 9 μm suggests that the bulk of the information contained in a series of images taken at different focal planes would be in planes of focus in that region.

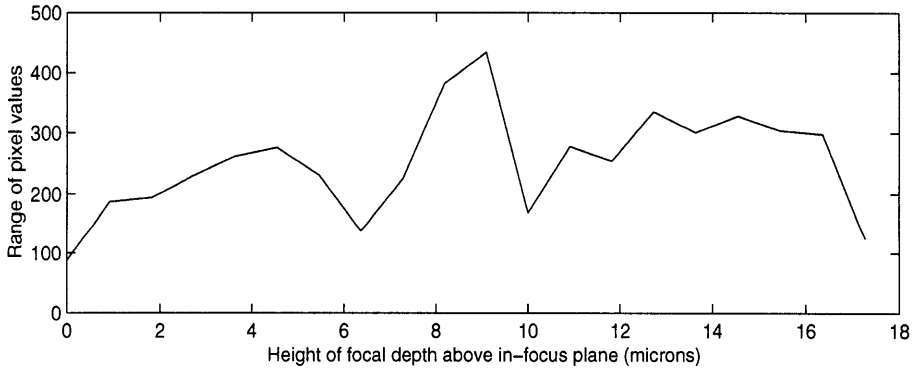

Figure 3.3: Range of pixel values in difference pictures versus distance from the in-focus plane. A high range value gives the indication that images taken at the corresponding plane of focus contain a good deal of information.

Another test involving the requisite range of depth was performed on the plastic diaphragm. I collected several volumes of images, varying the number of steps from 20 to 31 while keeping the step size fixed at 5/11 μm. Hence, I used a constant spatial sampling period of 5/11 μm with a range of depth that varied from 9.1 μm to 14.1 μm. I then com-

10. `sub`. See appendix A.

pared the magnitude and phase results at the fundamental and second harmonic for the various volumes. Figure 3.4 shows the results of this test. Using the constant step size, I found that the results were consistent throughout the tested range.

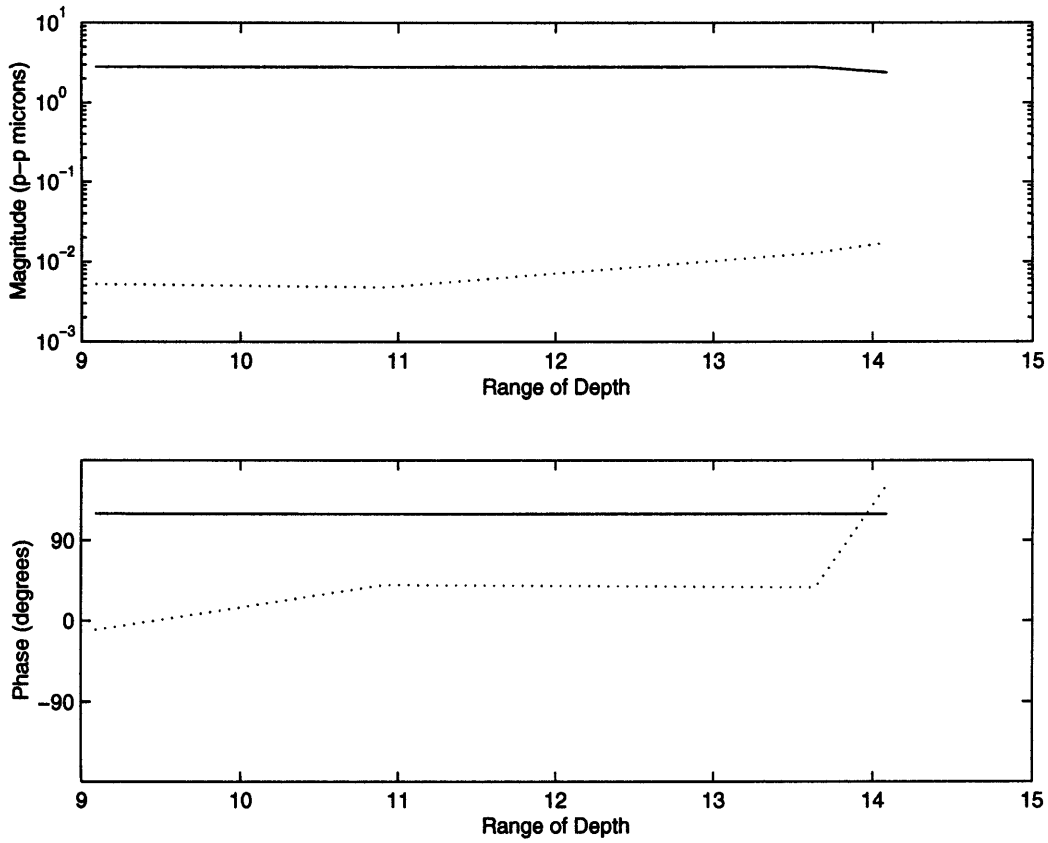

Figure 3.4: Displacement of plastic diaphragm vs. range of depth. Constant step size, varying range. Solid lines are fundamental; dotted lines are second harmonic.

While it is crucial not to undersample in the vertical direction, it is also important to avoid grossly oversampling by taking images at vertical steps too close to each other, both because the images are relatively large and take up computer hard disk space and because taking images with redundant information can greatly lengthen the image acquisition period.

I ran an experiment on the plastic diaphragm to test the importance of the number of steps used to span a constant range. I kept the range of depth at approximately 15 μm and varied the number of subdivisions from 8 to 31.

Figure 3.5 shows the results of the constant range of depth test. Shown are the z-directed magnitude and phase of five different combinations of step counts and step sizes that each cover a depth range of 15 μm. The results suggest that there is a significant difference in the z-motion estimate only for the experiment using 8 steps. If one describes the magnitudes of the higher harmonics as an indication of the noise floor, the test further indicates that the higher number of steps serves to lower the noise floor.

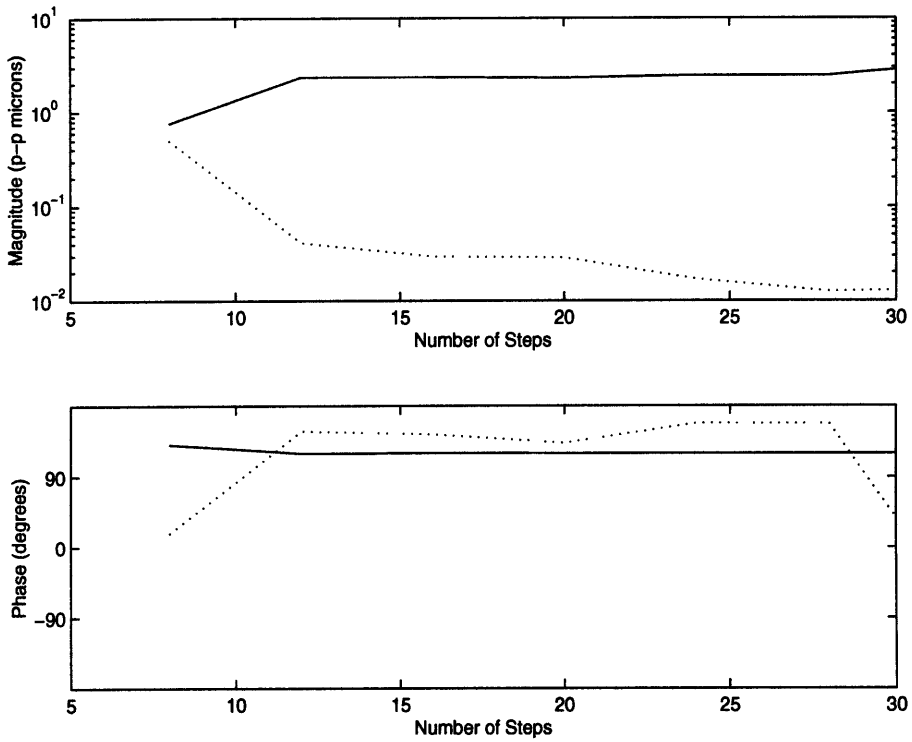

Figure 3.5: Reported magnitude and phase of motion vs. the number of steps used to span a constant range of depth. Solid lines indicate the fundamental frequency. Dotted lines indicate the second harmonic.

While previous experimenters have typically used 30 steps[11], the results of this resolution test indicate that in this case adequate motion estimates in the vertical direction can be obtained at resolutions as low as 16 steps. I found that for the motions of the plastic diaphragm, which are on the order of 1 μm, it seems to suffice to span approximately 15 μm with about 16 steps. The magnitude plot in figure 3.5 suggests that the only major differ-

11. Johnson (1997).

ence between 30 and 16 steps is the noise floor, but at 16 steps, the suggested noise floor is still two orders of magnitude below the measurement value.

For the bulk of my experiments on the plastic diaphragm, I used 28 steps of 6/11 μm each, but time constraints are more an issue in the temporal bone preparation, because of concerns about drying. Thus, I used 16 steps of 10/11 μm each for motion measurements on the temporal bone preparation. That change nearly halved the time spent acquiring each set of images.

Chapter 4

Results

Results from the human temporal bone preparation come primarily from two experimental sessions. The orientation of the preparation was slightly different in the two sessions. The second session served as a refining and a substantiation of the results from the first session.

The following four figures show the orientation of the stapes as viewed by the CCD camera and on what regions of the stapes the computer microvision measurements were focused. Figure 4.1 shows the defining characteristics of the stapedial head, as observed in the first experimental session. The two images in figure 4.1 show several identifiable elements of the stapes. On the right of the images is a portion of the stapedius tendon. The bottom of the images shows the stapedial head and the incudo-stapedial joint. The upper left region is the anterior crus, and the upper center gives a faint indication of the posterior crus. On the left image, I have drawn in the outline of the stapes to provide a less ambiguous sense of the orientation.

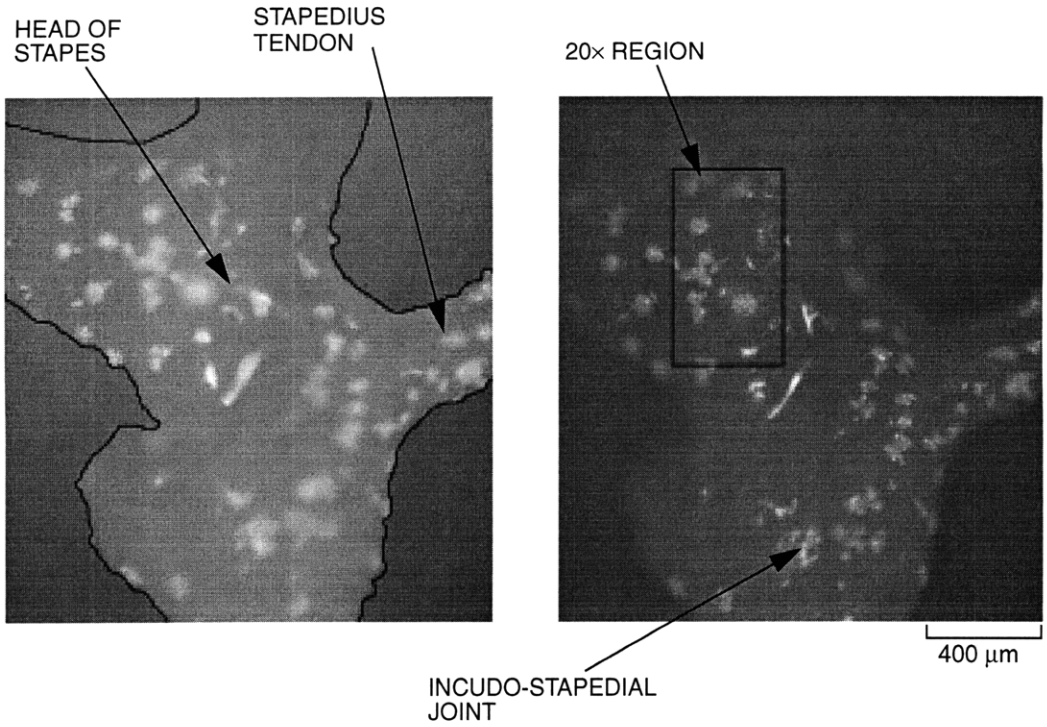

Figure 4.1: The head of the stapes. Left and right images show two different planes of focus. The rectangle in the right image corresponds to the area viewed under 20× magnification. The black outline of the stapes in the left image is my emphasis.

Figure 4.2 shows the region captured by the images used in the computer microvision measurements, which were taken using the 20× objective. This region corresponds to the rectangle in the previous figure with four times increased magnification.

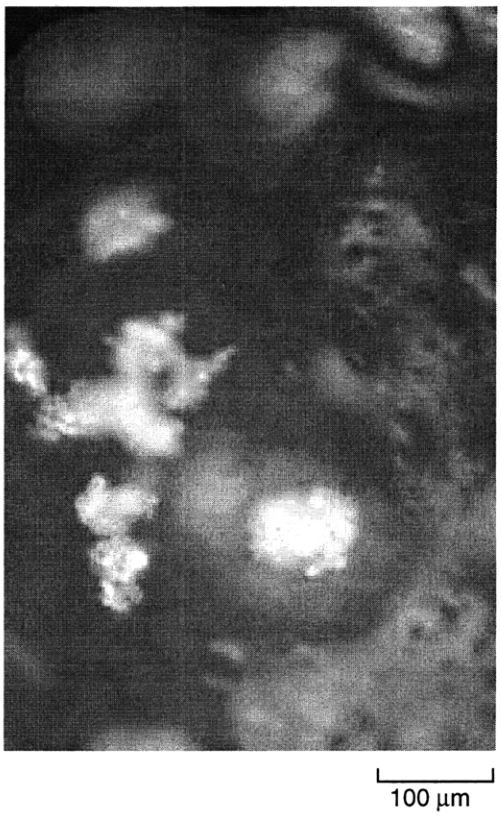

Figure 4.2: The head of the stapes, 20× objective. The inset axes indicate the x-, y-, and z- directions relative to the image.

The distinct bright spots are silver particles that provide a connection between images taken with the 5× and 20× objectives. Without them, it would be difficult to establish where on the stapes the 20× image focuses and what the important directions, such as the direction of piston-like motion, are relative to the image.

To simplify discussion of the orientation of the stapes, I define the angles ϕ and θ as in §3.2. Figure 4.3 applies these angles to sketches of the stapes. The angles represented in the sketch ($\phi = 115°$, $\theta = 105°$) are an estimate of the orientation of the stapes in the first experimental session.

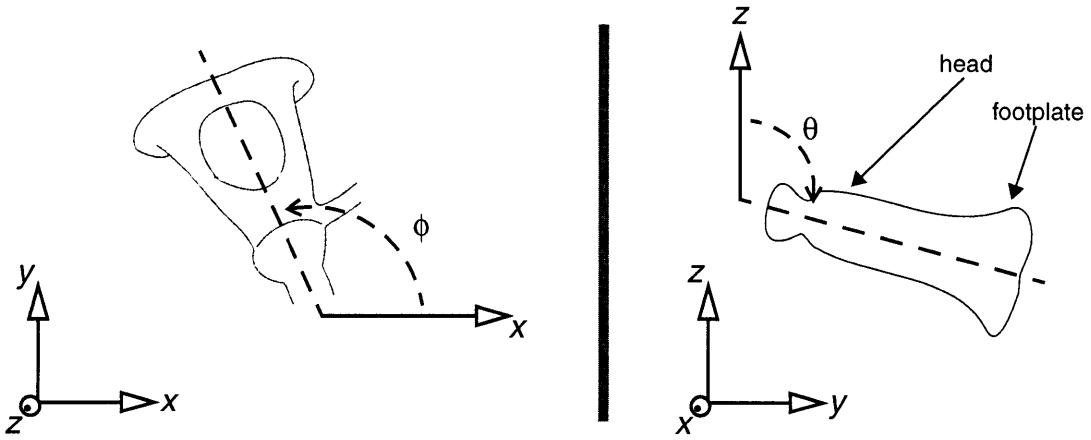

Figure 4.3: Definition of the angles ϕ and θ: the orientation of the stapes with respect to the coordinate system of the images. The right frame is a sketch of the stapes from the posterior view.

In the second experimental session, the specimen was oriented differently, such that ϕ and θ, the orientation angles of the stapes, were not the same as in the first experimental session. Also, fewer silver particles were placed on the stapes. Figure 4.4 shows the head of the stapes as viewed in the second session. The left image was taken using the 5× objective, and the right image using the 20× objective. That the stapes was at a somewhat steeper angle θ in figure 4.4 explains why less of the stapes appears in focus in the left image than in figure 4.1. The incudo-stapedial joint and the stapedius tendon are in view in the left image and serve as landmarks in determining the angle ϕ.

In both experimental sessions, the regions of interest were obtained by dividing the images into quadrants. That is, I divided the pictures into equal fourths by one line in the x direction and one line in the y direction.

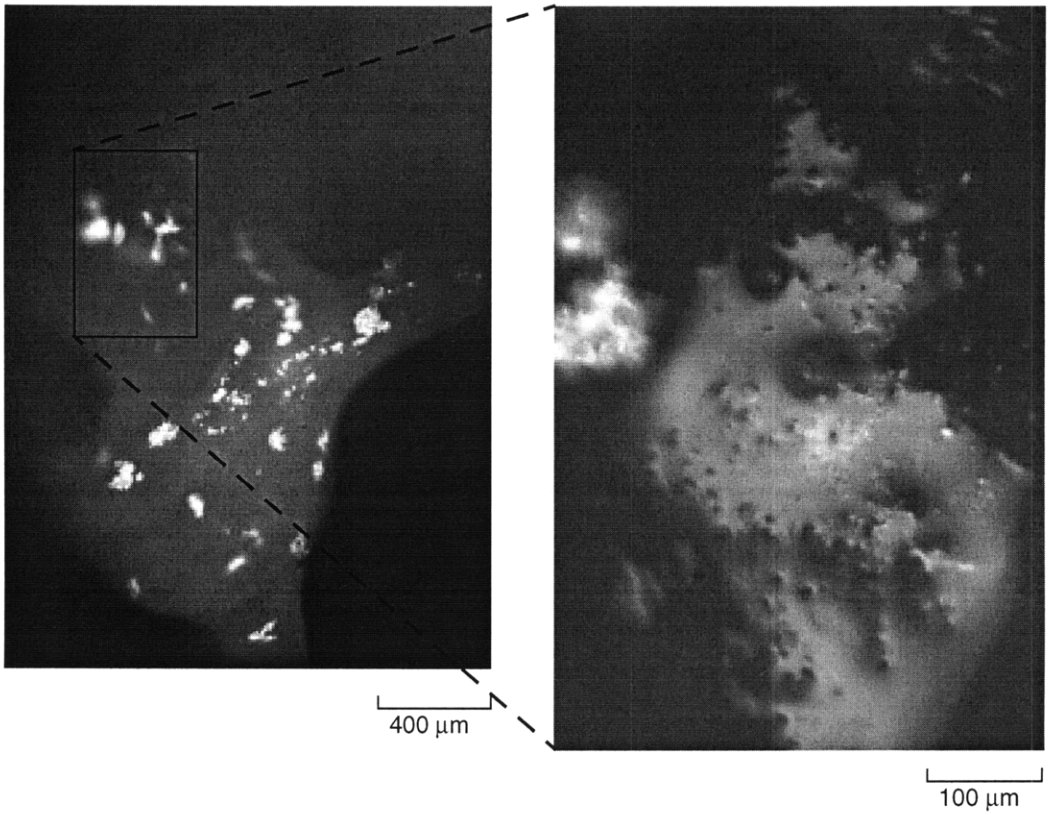

Figure 4.4: The head of the stapes. The left image was taken using the 5× objective. The right image was taken using the 20× objective. The rectangle in the left image corresponds to the entire right image.

4.1 Frequency Response

Leaving the DAC voltage constant at 50 mV, I measured the response of the stapes to sound pressures at the tympanic membrane which varied in frequency from 250 Hz to 6 kHz. At that DAC voltage, the magnitude of the sound pressure at the tympanic membrane varied with frequency as shown in figure 4.5. The sound pressure at the reference microphone is dependent upon the system which the transducer is driving. For instance, it is to be expected that the sound pressure would be significantly different when the transducer is coupled to the tympanic membrane than when it is freely driving in an open room. Because the coupling is likely air tight and because the tympanic membrane is within

5 mm of the reference microphone, the sound pressure at the microphone is a good estimate of the sound pressure at the tympanic membrane.

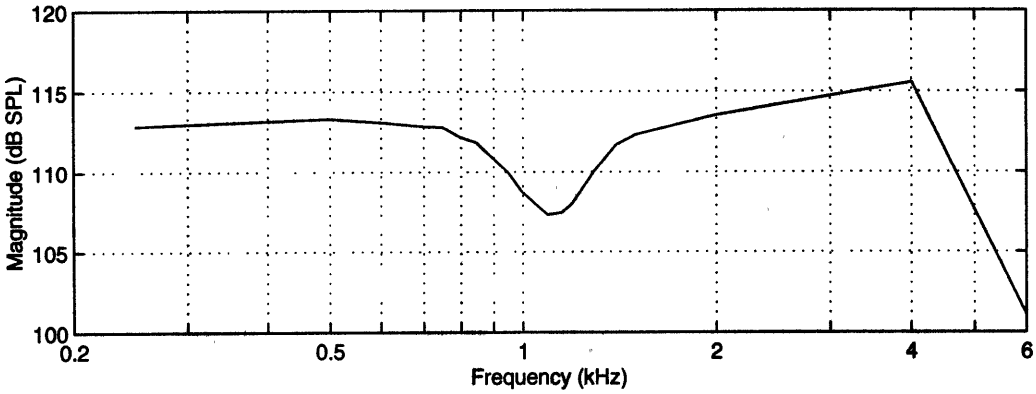

Figure 4.5: The sound pressure at the tympanic membrane vs. stimulus frequency while setting the output of the DAC at 50 mV. Most of the sound pressures lie within an 8 dB range.

Figure 4.6 is the plot of stapes displacement versus frequency obtained from the first experimental session. Shown are the magnitude and phase components of the fundamental frequency of stapes displacement in the x, y, and z directions. Because the measurements were made at varying SPLs, results are given normalized to the sound pressure at the tympanic membrane. The data illustrate that the magnitude of the y component of the measured motion is a factor of 2-3 larger than the z component and a factor of 10-30 larger than the z component. Also, while y and z components are in phase with each other, they are roughly 180° out of phase with the x component. Each graph contains a plot of the individual ROIs and the similarity of the motion of these areas adds credence to the measurement analysis and also suggests that the measurement rectangle outlines a rigid structure.

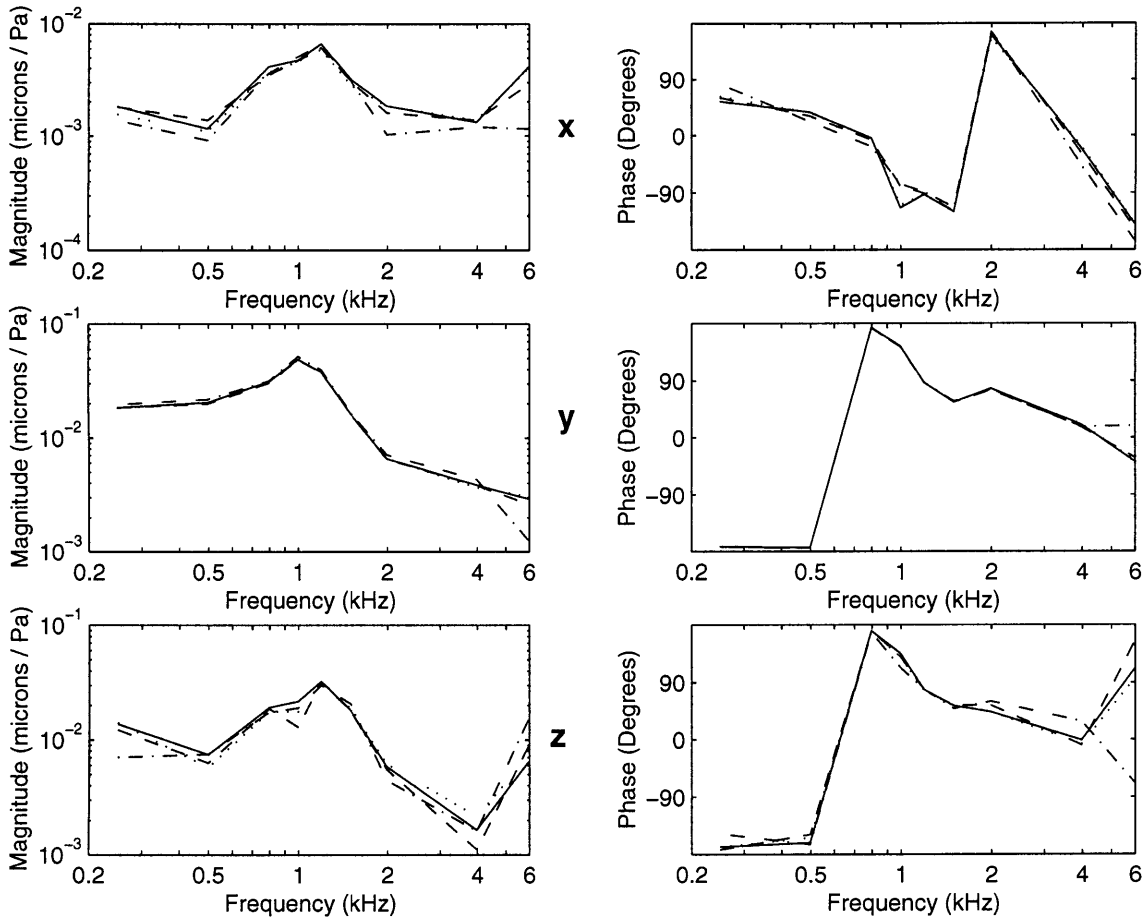

Figure 4.6: Frequency response of the human temporal bone preparation, first session: x-, y-, and z-directed motion, normalized to sound pressure at the tympanic membrane. Each curve on the figure shows the motion of an individual ROI.

The directional analysis derived in §3.2 yielded a frequency response with respect to the major and minor axes of motion. Figure 4.7 shows fundamental frequency stapes motion along the major direction, $\hat{\imath}_m$. Again, the magnitudes are normalized to the sound pressure at the tympanic membrane and the phase measurements are relative to the phase of the sound pressure at the tympanic membrane.

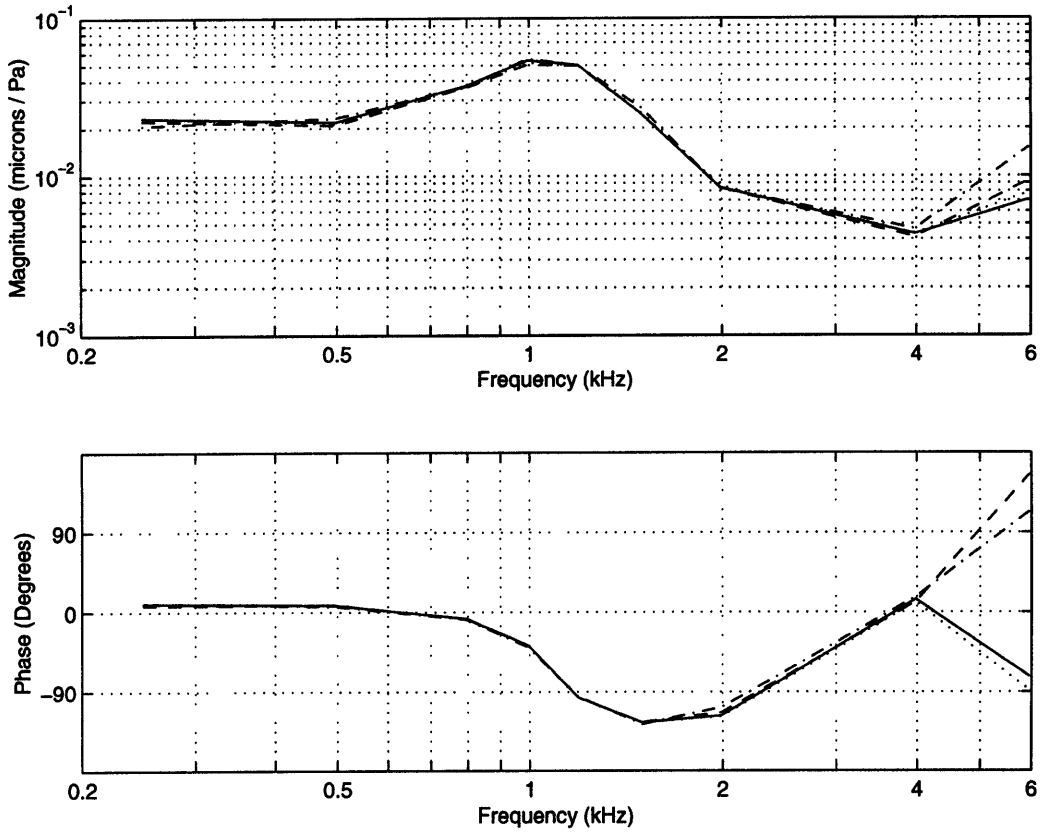

Figure 4.7: Motion along major axis, normalized to sound pressure. The magnitude and phase of primary direction motion at the fundamental frequency vs. stimulus frequency. First experimental session. Each line corresponds to one of four different ROIs.

Similar to the feline stapes results by Guinan and Peake, there appears to be a resonant frequency of approximately 1 kHz followed by a sharp drop-off in magnitude. For frequencies below 800 Hz, there is zero phase between the displacement of the ossicles and the applied sound pressure.

Figure 4.8 shows the minor-direction component of the frequency response from the first experimental session. The phase of the displacements along the minor axis is generally the phase along the major axis minus 90°; this result is a confirmation that the directional analysis is working properly–that the axes along which figures 4.7 and 4.8 have been defined are the major and minor axes, respectively, of the fundamental frequency.

That the magnitude of motion along the major axis is a factor of 5-20 times larger than the minor-axis component suggests that motion is well described by simple translation. Such a translation is also consistent with the observations of in-phase behavior of the larger motions in the x-y-z coordinate system.

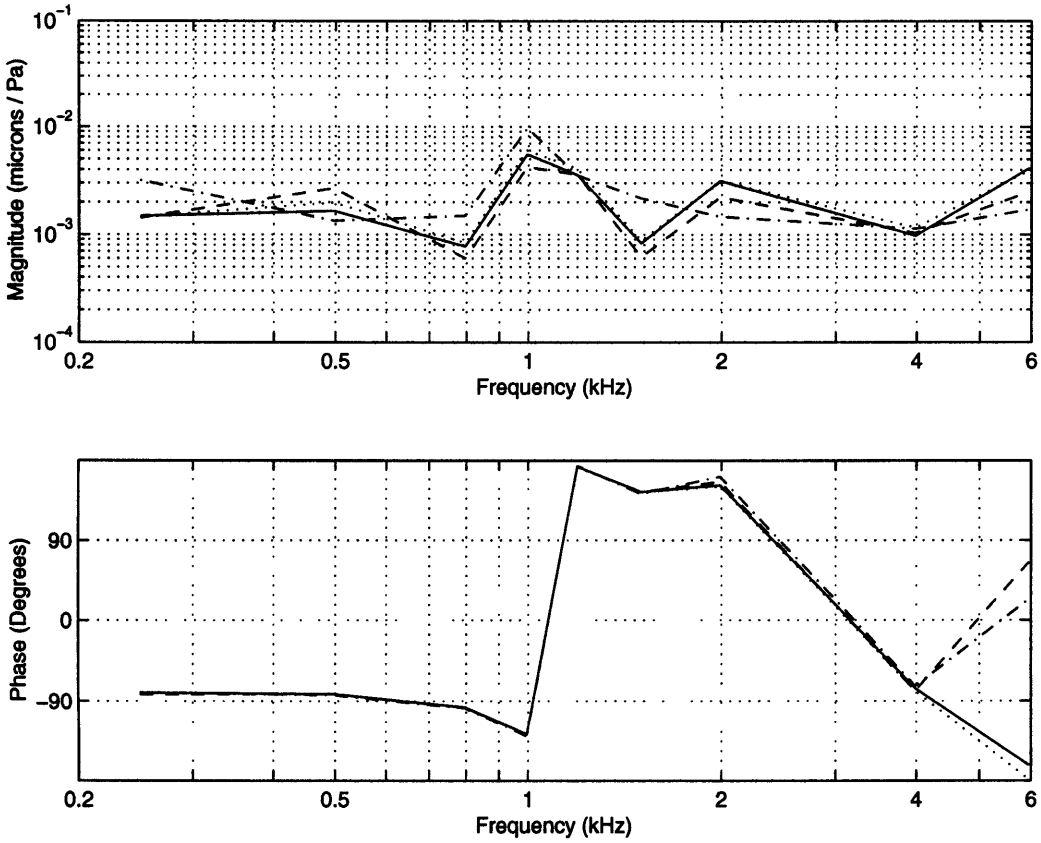

Figure 4.8: Motion at fundamental frequency along minor axis, normalized to sound pressure. First experimental session. Four different ROIs.

The bone was at a somewhat different angle in the second experimental session, and the stimulus frequency was varied from 250 Hz to 2 kHz, with higher resolution around the apparent pole at 1 kHz. The results from the second experimental session seem to coincide with those from the first. Figure 4.9 shows the x-, y-, and z-directed displacements obtained from the second session. These data again show that the y component of the motion was largest in magnitude. However, in this session, the next largest motion component was in the x direction. In general, the z-directed magnitudes appear small and the

magnitudes and phases of this component appear noisy. As in the first session, the angles of the x and y components are out of phase, while the y and z components are roughly in phase.

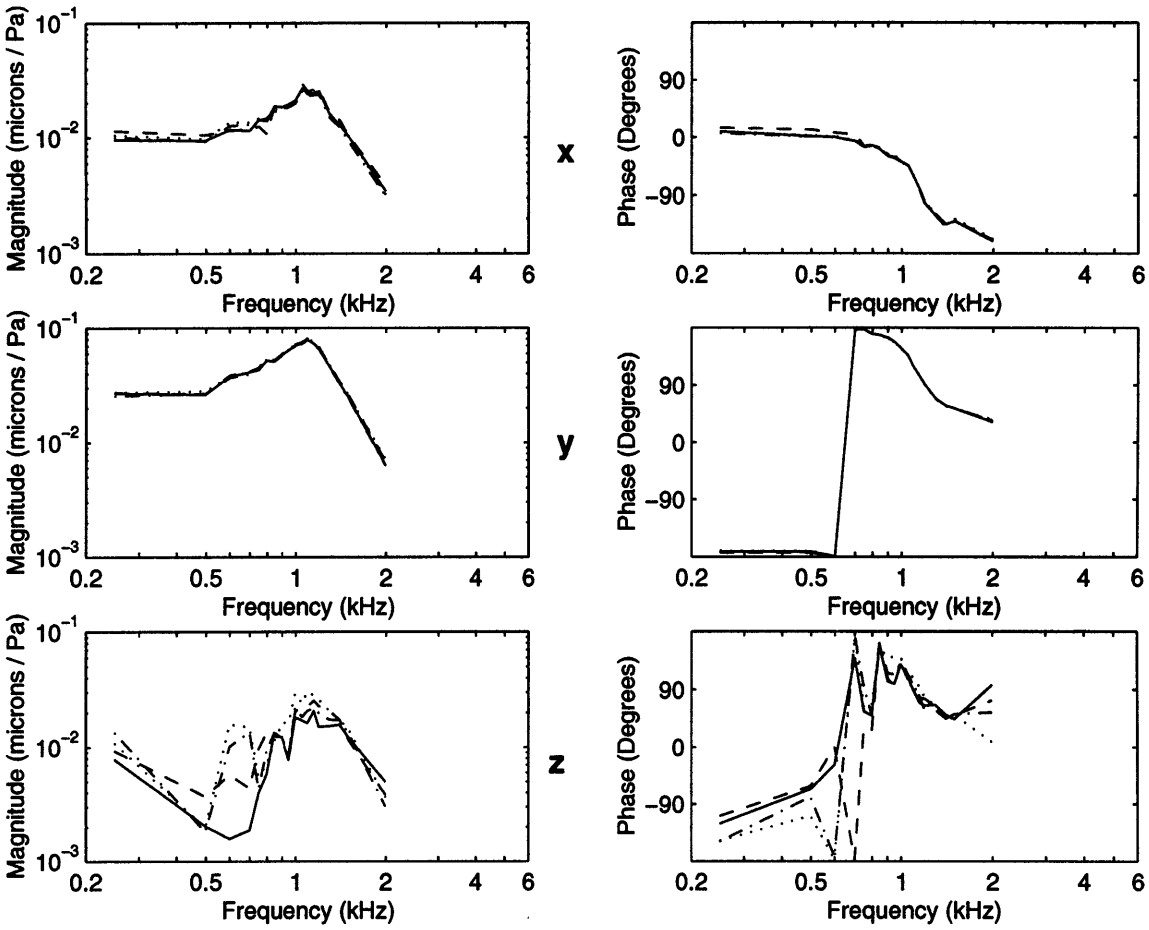

Figure 4.9: Frequency response of the human temporal bone preparation, second experimental session: x-, y-, and z-directed motion, normalized to sound pressure at the tympanic membrane.

Figure 4.10 shows the major axis component of fundamental frequency stapes motion from the second session. Due to the higher frequency resolution in the 1-kHz range, it is apparent from figure 4.10 that the resonance point is approximately 1.1 kHz.

The frequency response plots of major-axis displacement from the first and second sessions have similar characteristics. The magnitude is constant for frequencies below 500 Hz. The response reaches a peak at 1.1 kHz, after which the magnitude falls off rap-

idly. Such behavior is indicative of a pole in the system. For frequencies below 800 Hz, the displacement along the major axis and the sound pressure at the tympanic membrane are roughly in phase.

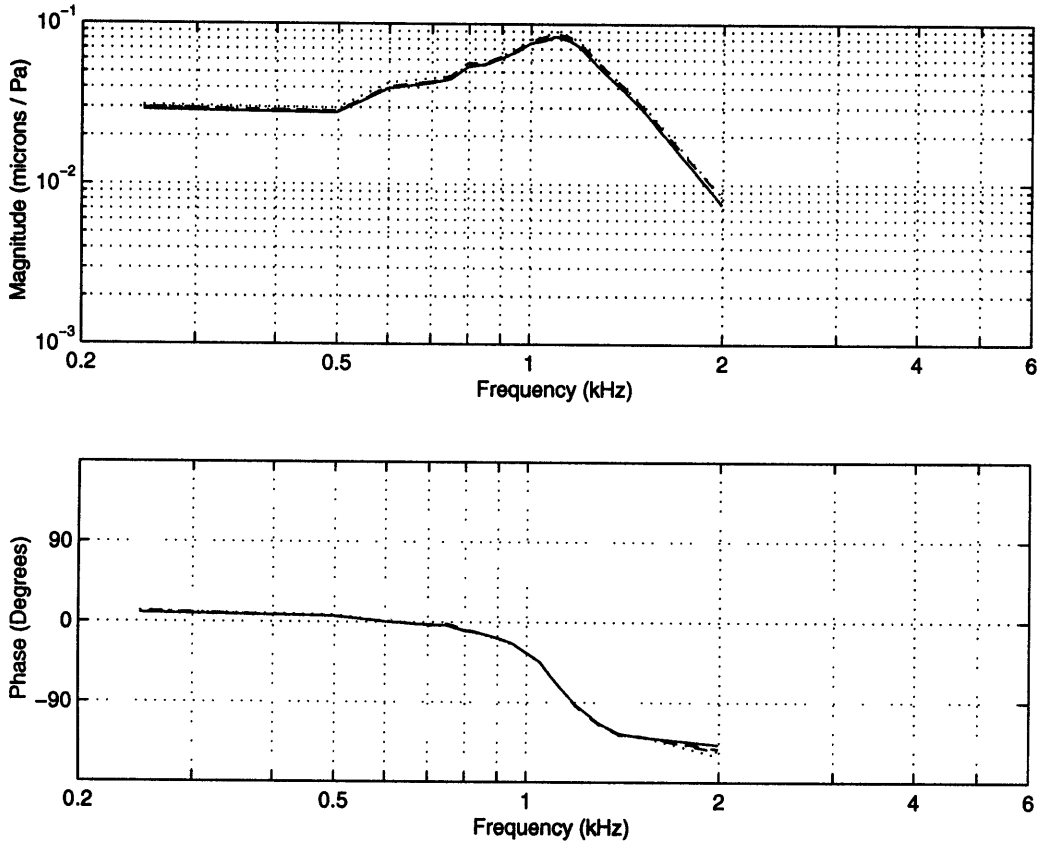

Figure 4.10: Displacement along major axis of motion, fundamental frequency: second experimental session.

Figure 4.11 shows the minor-axis displacement at the fundamental frequency. Once again, these displacements are 3-10 times smaller in magnitude than those along the major axis, and the phase angle lags that of the major axis by 90°.

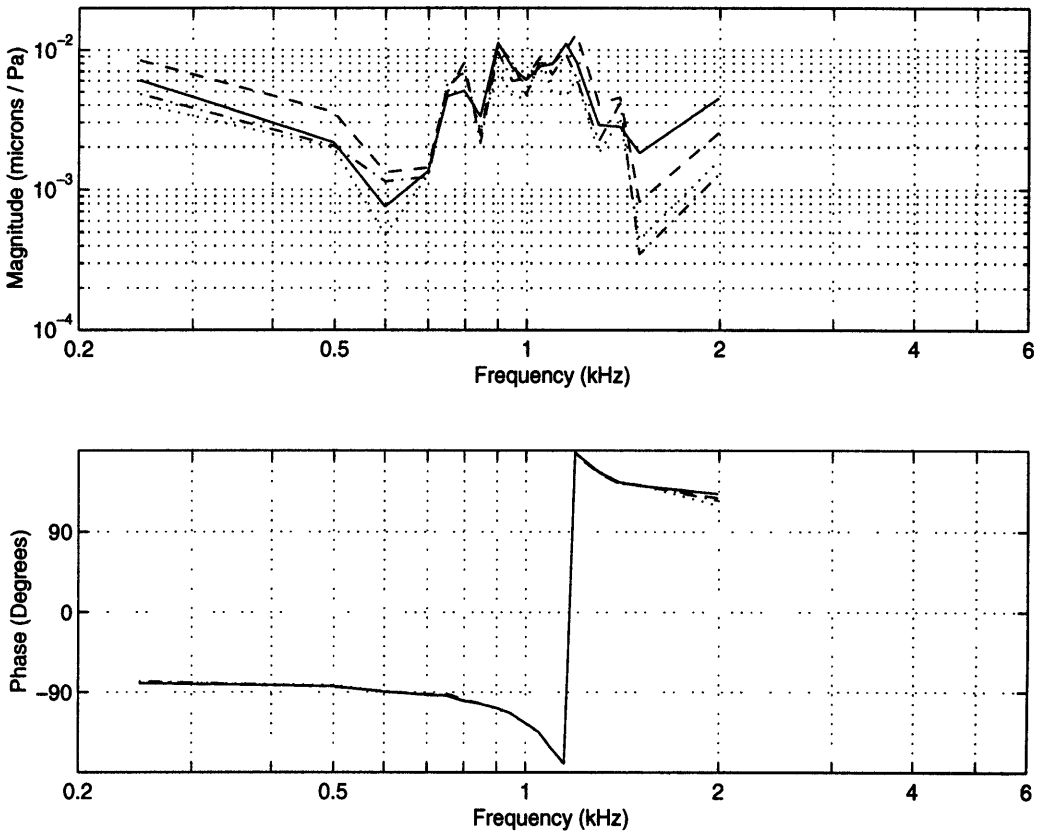

Figure 4.11: Displacement along minor axis, fundamental frequency component: second experimental session.

4.2 Linearity and Reproducibility

The primary indicator of the linearity of a system response being measured with computer microvision is the reported magnitudes of the higher-order harmonics. Since complex exponentials are eigenfunctions of linear systems, a sinusoidal input of a given frequency will produce in a linear system an output which is some scaled, shifted version of the original sinusoid. It is characteristic of nonlinearities that a sinusoidal input of one frequency can produce an output with varied frequency content. Because measurement noise can also appear as higher-order harmonics, the magnitudes at frequencies other than the fundamental can be interpreted either as a quantification of the nonlinearity in the stapes

response or as an indication of the noise floor of my measurements–a measure either of linearity or reproducibility.

As a control in the second experimental session, I made repeated measurements at 500 Hz in order to investigate the time evolution of stapes response. Figure 4.12 shows the magnitude results of those measurements plotted versus the time from the beginning of the session.

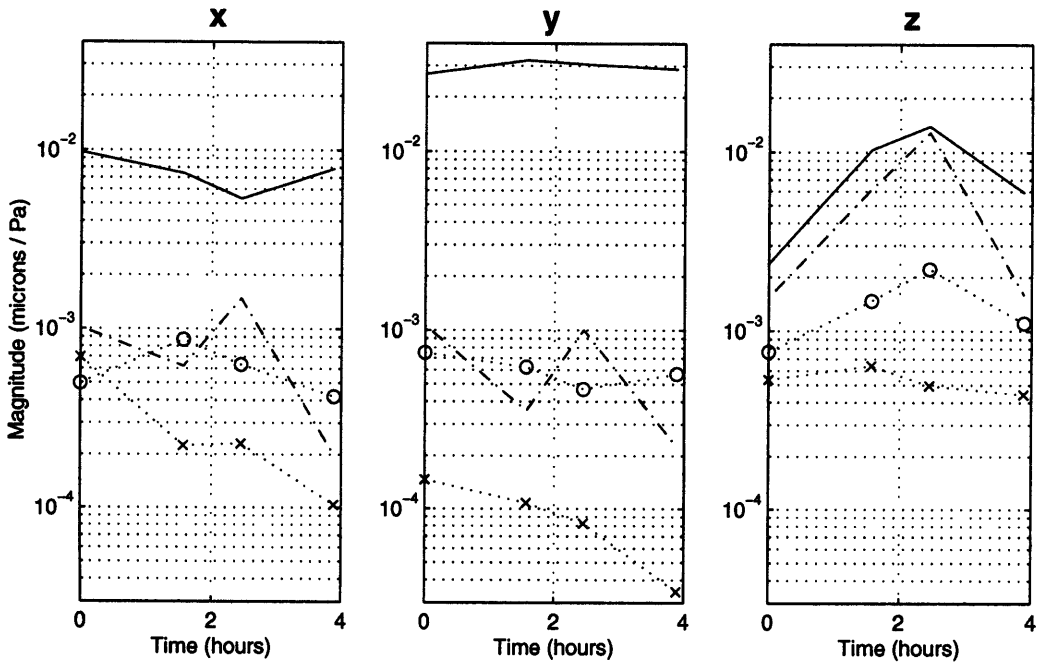

Figure 4.12: Mean and standard deviation of fundamental and second harmonic motion magnitudes in the x, y, and z directions vs. time from the first measurement. The stimulus frequency was 500 Hz. Fundamental: solid lines are the mean of four ROIs, circles are the standard deviation. Second harmonic: dashed lines are mean, x's are standard deviation. From the second session.

The three plots in figure 4.12 carry a good deal of significance. They give information concerning the linearity of the stapes response, the reproducibility of motion estimations from a single set of images, and the time course of the stapes response. In the case of the x and y directions, the circles appear on average at about the same value as the dashed lines. That the standard deviation of fundamental-frequency estimates and the mean of second-harmonic measurements are approximately the same is a strong indication that the noise

floor lies in that range. Due to microscope symmetry, it is to be expected that the same noise floor should hold for both the x and y directions.

In the case of z-directed motion, it is apparent that the estimates are far noisier than in the case of the other two directions. In general, the second-harmonic z magnitude is almost as great as that of the fundamental, which could suggest that the response in the z direction is highly nonlinear.

4.3 Direction

If it can first be established that motion is translational, a further step toward confirming the hypothesis that stapes motion can be characterized as piston-like requires understanding the direction in which the major component lies. A measure of the degree to which stapes motion is translational in some direction is the ratio between the magnitudes of motion in the major $\hat{\imath}_m$ and lesser $\hat{\imath}_l$ directions. This ratio indicates how much greater is the length of the elliptical path than its width. Figures 4.13 and 4.14 are plots of the ratio between the magnitudes of motion along the major and minor axes for the first and second experimental sessions, respectively. The ratio between the major and minor axes appears similar between the two sessions, even though the overall magnitude of the motions from the second experimental session are approximately twice as large as those from the first.

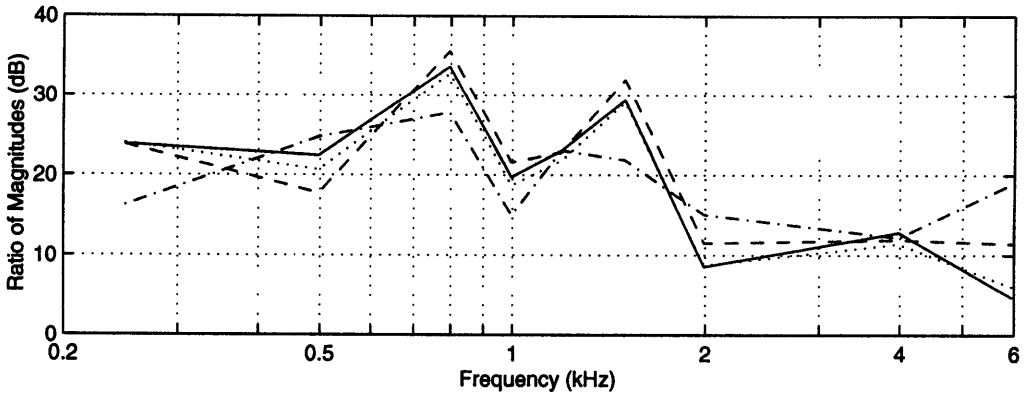

Figure 4.13: Ratio, in dB, of the major- and minor-axis magnitudes for the first experimental run vs. frequency.

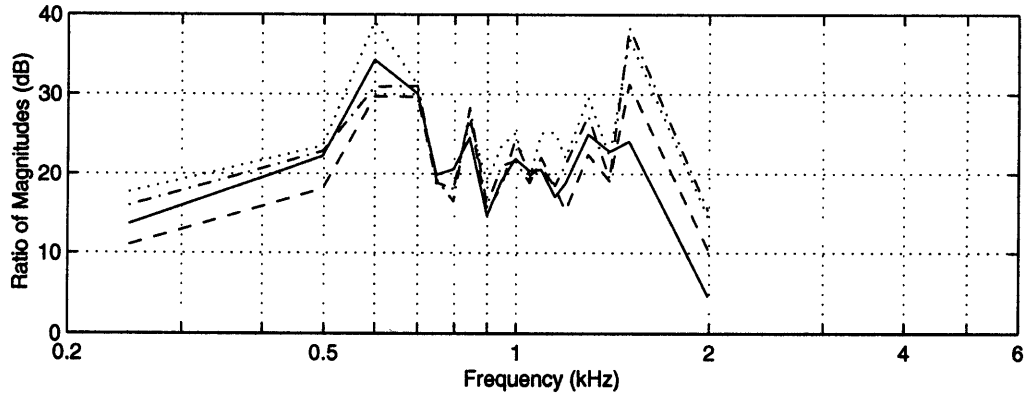

Figure 4.14: Ratio of the major- and minor-axis magnitudes for the second experimental run vs. frequency.

The data analysis which produces the magnitude and phase plots along the major and minor axes also yields the direction of major-axis translation in terms of the coordinate system of the images (x,y,z). The orientation angles ϕ and θ are as defined at the beginning of the chapter.

Figure 4.15 shows the frequency dependence of the angle ϕ for both experimental sessions. Squares indicate data points for individual ROIs in the first session. Circles indicate data points for individual ROIs in the second session. For frequencies 2 kHz and below, the estimates of ϕ between ROIs in a session seem consistent with each other–likely more consistent than any visual estimate I would be able to make of the orientation of the stapes.

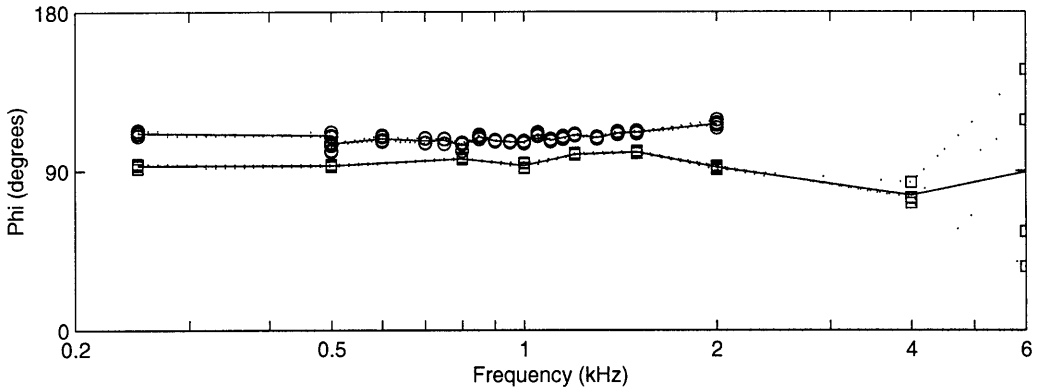

Figure 4.15: The angle ϕ of the major axis vs. frequency. Squares indicate results from the first session. Circles indicate results from the second session. At 500 Hz, circles indicate four ROIs at each of four time-separated measurements.

Figure 4.15 also suggests that ϕ remains constant throughout the 250 Hz to 2 kHz range, although the angles in the first and second sessions remain constant at different values.

Figure 4.16 is a similarly devised plot of the orientation angle θ for four ROIs in each of the two experimental sessions. The reported values of θ vary more among ROIs and with frequency than the corresponding values of ϕ seen in the previous figure.

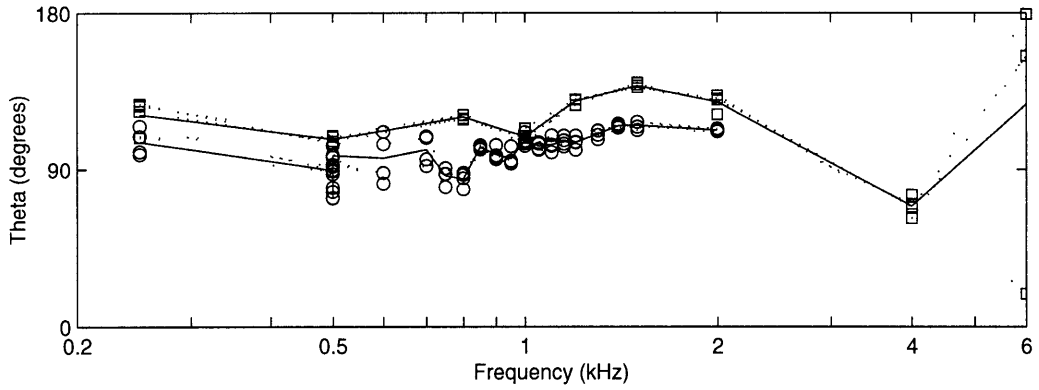

Figure 4.16: The angle θ of the major axis versus frequency. Squares indicate results from the first session. Circles indicate results from the second session. At 500 Hz, circles indicate four ROIs at each of four time-separated measurements.

Referring back to figures 4.6 and 4.8, it is apparent that variance in θ is largely due to variance in z-directed motion. The angle ϕ is unaffected by the variance in the z direction, because it is calculated solely from motion in the x and y directions.

Because the magnitude and phase along the major axis agree in all four ROIs and between sessions (figures 4.7 and 4.10), and because the orientation angles ϕ and θ are somewhat consistent within sessions, it is suggestive that stapedial motion has a strong translational component which is compliance dominated for frequencies below resonance.

However, because the ratio between major- and minor-axis motions is not so large as to declare minor-axis motion insignificant, these results cannot completely rule out the possibility of some rocking component to the motion of the stapes in this temporal bone preparation.

Chapter 5

Discussion

5.1 Stapes Translation

For frequencies from 250 Hz to 2 kHz and sound pressures around 110 dB, my results indicate that the stapes in this temporal bone preparation is translating.

The sets of raw data presented in figures 4.6 and 4.9 suggest that the motion of the stapes in this preparation is primarily translational. The x, y, and z components of the motion are generally either in phase or 180° out of phase, and the magnitudes evolve similarly with frequency.

Translation is also apparent from the ratio between the major- and minor-axis amplitudes in either experimental session. While figures 4.13 and 4.14 suggest the presence of some minor-axis component to the motion, those magnitudes are relatively small. If some large rotational component were present in the system, I would further expect the magnitude and phase along the major axis, as well as the calculated direction of translation of that axis, to vary greatly among regions of interest. That is simply not the case.

5.2 Comparison with Laser Response

As a reference against which to compare computer microvision measurements, a unidirectional measurement of the stapedial motion in this temporal bone was made using a laser doppler vibrometer. The results of those measurements are shown in figure 5.1, a plot analogous to figures 4.7 and 4.10. Figure 5.1 confirms the general shape of the previous magnitude and phase plots, but the magnitudes are considerably smaller in figure 5.1. This

discrepancy is at least in part due to the orientation of the stapes in the laser measurements.

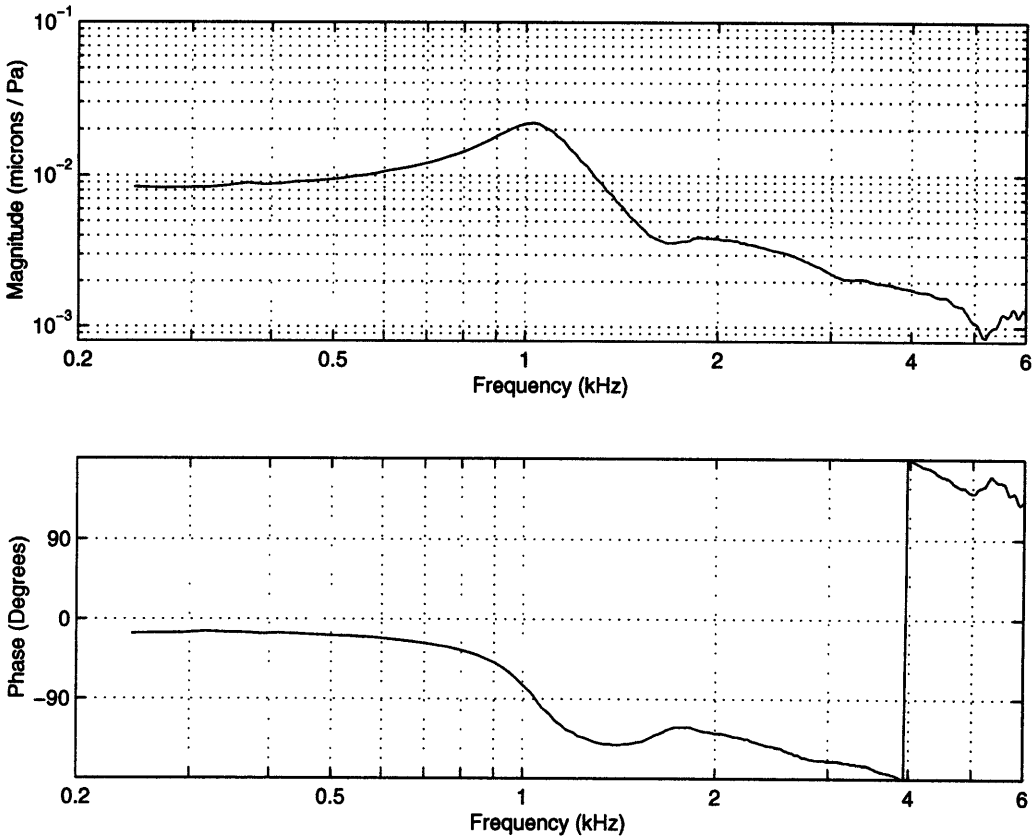

Figure 5.1: Frequency response of stapes displacement. Data collected using a laser-doppler vibrometer.

The phase indicated in figure 5.1 is also consistently approximately 20° lower than the corresponding values from figures 4.7 and 4.10. Note, however, that in figure 3.2, the results from the same laser system also had phase that was approximately 20° lower than the phase obtained from my computer microvision estimates. It must be wondered whether there is some persistent error either in the computer microvision or laser doppler calibrations.

5.3 Direction of Piston-like Motion

Because computer microvision can simultaneously measure motion in three dimensions, I was able to calculate the direction in which the stapes translated. Such a calculation would have been impossible or extremely difficult with unidirectional measurements. A natural limitation to my ability to confirm whether stapedial motion is piston-like is the ability to estimate the orientation angles of the stapes. In figures 5.2 and 5.3 below, I replot the angles from figures 4.15 and 4.16 atop sketches of the stapes oriented as my estimate of the stapes in the temporal bone preparation.

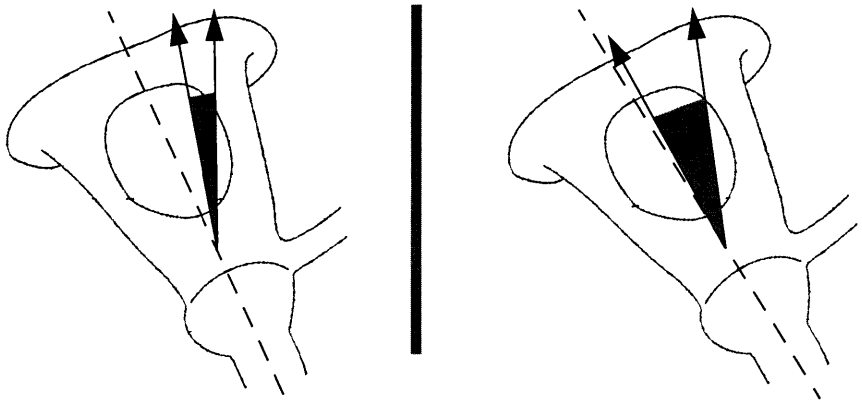

Figure 5.2: Range of the orientation angle ϕ of the major axis of stapedial motion, plotted atop a sketch of the stapes. Left is the first experimental session, oriented at $\phi = 115°$ and only for frequencies 2 kHz and below. Right is the second session, oriented at $\phi = 120°$.

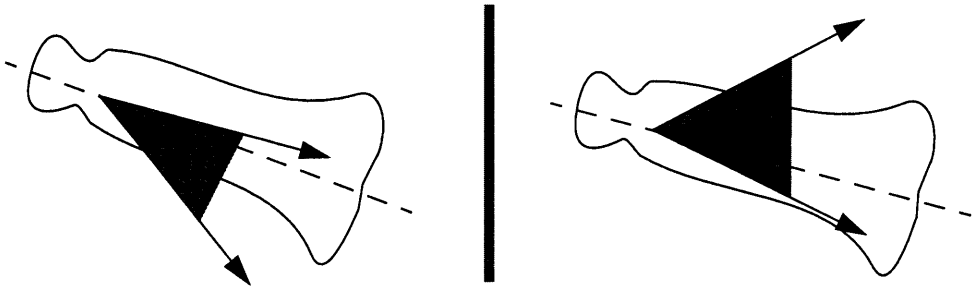

Figure 5.3: Range of the orientation angle θ of the major axis of stapedial motion, plotted atop a posterior-view sketch of the stapes oriented at $\theta = 105°$. Left is the first session, only for frequencies 2 kHz and below. Right is the second session.

Referring back to figures 4.15 and 4.16, it appears that most of the variance in the angles comes from frequency dependence rather than from measurement variance. In the above figures, I have oriented sketches of the stapes from the first and second sessions with the same θs but with differing ϕs. A method of more precisely estimating the orientation of the stapes would greatly assist an interpretation of the axis of translation.

5.4 Conclusions

Computer microvision has great potential for answering the question of the nature of stapedial motion as well as can be addressed with human cadaver material. While my results can only suggest how the stapes in this temporal bone moves and thus do not have great value in establishing a characterization of stapedial motion in live humans, the main benefit is the suggestion that computer microvision can indeed be useful in future stapedial motion measurements.

The strong advantage of computer microvision in comparison to other systems is that the experimenter can look at exactly what is being measured. Objectives with lower magnification can be used to assure the experimenter of what exactly is in view. Furthermore, one set of pictures can lead to three-dimensional motion measurements of several rigid-body structures simultaneously in view of the camera.

As a measurement system for use on the human temporal bone, computer microvision is not without disadvantages. It takes considerably more time to acquire a volume of images for use in computer microvision analysis than it would to acquire data from a laser-doppler vibrometer. Moreover, the stapes is within the temporal bone at a depth nearly equal to the working distance of the microscope objectives, making it difficult to position the preparation so that much of the stapes is in view of the microscope.

Further measurements of stapedial motion should be performed on several fresh temporal bones. It must be noted that the human temporal bone preparation I used was not in an ideal condition. The preparation was at least a year old, and the inner ear had likely been drained of all fluid. The bone's primary utility was as a preliminary target used to explore complications related to this new application of computer microvision before moving on to a specimen more apt to provide reliable data.

It would also be useful to perform measurements at various physiological sound pressure levels. As reported in figure 4.4, the range of sound pressures I used lay between 100 and 116 dB. While those SPLs are below the threshold of pain, they certainly lay at the upper end of what could be considered near-normal sound pressures. Through mechanical arguments, Békésy suggested two different modes of motion for higher and lower sound pressures, and his dividing line between the two was the threshold of hearing. Measurements at lower sound pressures could establish whether there is such a change in the mode of stapedial motion. Crucial to measurements at lower levels, however, would be a lowering of the noise floor, which was high in my estimates of vertical motion.

Several factors could contribute to measurement noise in the z direction. A likely interpretation is that the conclusions from my method tests (See again figures 3.3 and 3.4.) are in some way wrong, and I was either undersampling in the z direction or I was not covering a deep enough vertical range. Accurate estimates of the requirements for these measurement parameters would be important to any future stapes measurements.

Appendix A

Command Descriptions

The following are descriptions of some command-line programs I used in the acquisition and processing of computer microvision data.

```
fft infile mag outfile
```

This program takes the fast Fourier transform of a picture (e.g. a properly cropped image from a volume) that has dimensions which are some power of 2. It writes the output to *outfile*.mag and *outfile*.phase. These output files are themselves pictures. In the center of the *outfile*.mag picture is the magnitude of the spatial-frequency DC component in the x and y directions of the original picture. Along the increasing x-axis are the magnitudes at increasing x-directed frequencies. Along the increasing y-axis are the magnitudes at increasing y-directed frequencies. Since the images I fed the program are real-valued, I expect the *outfile*.mag images to have quadrantal symmetry.

```
ledslomo stim_volt stim_freq LED_freq
```

The light source and the stimulus are driven by different channels on the DAC. This command drives the stimulus channel at *stim_volt* mV and *stim_freq* Hz while dirving the LED channel at *LED_freq* Hz. Using a difference of 1-3 Hz between the two frequencies, the command produces a strobe effect that slows the apparent motion of the subject to frequencies visible to the human eye. No output files are generated.

```
ledvol -stage [-ledtime time] outfile #pics/zpos
#zpos stepsize voltage freq
```

This command is used to obtain a volume of images while stimulating the subject. The program takes a picture at each of *#pics/zpos* phases of the stimulus waveform. Such a set of images is taken at a total of *#zpos* planes of focus, each separated by *stepsize* μm. The image acquisition begins at the in-focus plane of the subject and then the stage moves downward, resulting in a plane of focus higher on the subject. Synchronized to the pulsing LED, which provides the lighting for the images, is the stimulus at *voltage* mV and *freq* Hz. The optional -ledtime switch changes the total LED duration (an integral multiple of the length of the individual LED pulse) from its default of 62 ms to *time* ms. The output pictures are all named *outfile* with some suffix.

```
vol -stage outfile #pics stepsize #avgs
```

This program takes a static volume of images similarly to the manner in which ledvol operates. No stimulus is involved, so only one image is taken at each of *#pics* focal planes separated by *stepsize* μm each. Further, each output picture is the produce of average of *#avgs* individual images.

```
sub image1 image2 difference
```

This routine calculates the difference image. Each pixel value in *difference* is the corresponding value in *image1* minus the corresponding value in *image2*. Thus, in the difference image, dark regions are areas where the two original images are similar and bright areas are where they heavily contrast.

```
2ptnormcrpr3dflow -nonorm outdir magnification
stepsize phases_per_plane roifile back dark
input_pics ...
```

This command performs the two-point correction using background picture *back* and the dark pictures *dark*, crops the images according to the specifications in *roifile*, and then uses the motion estimation algorithms. The user specified the microscope *magnification*, the *stepsize* between planes of focus, and the number *phases_per_plane* of phases during a stimulus period at which pictures were taken. The input images *input_pics* are given in the order in which the `ledvol` program numbered them. The program outputs cropped, corrected pictures and motion files in the *outdir* directory. The `-nonorm` option avoids normalizing the pictures to a common average. Normalization was necessary for a previous version of computer microvision which featured a strobe lamp instead of an LED.

Appendix B

MATLAB Script

The following is my MATLAB script for reorienting FFT data in terms of the major and minor axes of the motion at the fundamental frequency.

```
function [new,phi,theta]=primary(data)

%function [new,phi,theta]=primary(data)
%Function to find components in new coordinate system where m is the
%primary or major direction of motion, l is the lesser direction of motion, and n
%is the null direction (no fundamental).
%phi and theta describe in standard spherical coordinates the m direction
%in terms of the x,y,z coordinate system.
%data is the data matrix

% data is a 3-D array:
% first index indicates harmonic number
% second index indicates mag (1) or phase (2)
% third index indicates x, y, or z.

% Calculates the phase lag of y and z relative to x (in radians)
ylag = (data(1,2,2)-data(1,2,1))*pi/180;
zlag = (data(1,2,3)-data(1,2,1))*pi/180;

% Assuming now that the position d-> is of the form:
% d->(t) = x cos(t) x^ + y cos(t+ylag) y^ + z cos(t+zlag) z^
% then the maximum and minimum amplitudes are at time t, t+90
x2 = data(1,1,1)^2;
y2 = data(1,1,2)^2;
z2 = data(1,1,3)^2;
s2y = sin(2*ylag);
s2z = sin(2*zlag);
c2y = cos(2*ylag);
c2z = cos(2*zlag);

num = y2*s2y + z2*s2z;
denom = x2 + y2*c2y + z2*c2z;
t = -atan2(num,denom)/2;

% Now, figure out which of the two is the max and which is the min.

mag1 = x2*(cos(t))^2 + y2*(cos(t+ylag))^2 + z2*(cos(t+zlag))^2;
mag2 = x2*(cos(t+pi/2))^2 + y2*(cos(t+pi/2+ylag))^2 + z2*(cos(t+pi/2+zlag))^2;

% Wait on case where there is only one direction of motion

if abs(log(mag1/mag2)) < 25
       if mag1 > mag2
       tmax = t;
       tmin = t+pi/2;
       else
       tmax = t+pi/2;
       tmin = t;
```

```
      end

% Now I have vectors in the m and l directions.
% They are the value of d->(t) at tmax and tmin, respectively.
% The direction of zero amplitude (n) is simply l x m.
% Define the matrix that transforms any x,y,z point into l,m,n coordinates.

xyz2m = [data(1,1,1)*cos(tmax) data(1,1,2)*cos(tmax+ylag)
data(1,1,3)*cos(tmax+zlag)];
xyz2lmnmag = sqrt(xyz2m(1)^2 + xyz2m(2)^2 + xyz2m(3)^2);
xyz2m = xyz2m/xyz2lmnmag;
xyz2l = [data(1,1,1)*cos(tmin) data(1,1,2)*cos(tmin+ylag)
data(1,1,3)*cos(tmin+zlag)];
xyz2lmnmag = sqrt(xyz2l(1)^2 + xyz2l(2)^2 + xyz2l(3)^2);
xyz2l = xyz2l/xyz2lmnmag;
xyz2n = [xyz2l(2)*xyz2m(3)-xyz2l(3)*xyz2m(2) xyz2l(3)*xyz2m(1)-xyz2l(1)*xyz2m(3)
xyz2l(1)*xyz2m(2)-xyz2l(2)*xyz2m(1)];

xyz2lmn = [xyz2l ; xyz2m; xyz2n];

% Its inverse is the matrix that transforms any (l,m,n) to (x,y,z).
lmn2xyz = inv(xyz2lmn);

cy = cos(ylag);
cz = cos(zlag);
sy = sin(ylag);
sz = sin(zlag);
x = data(1,1,1);
y = data(1,1,2);
z = data(1,1,3);

% Now, I want to calculate a and b for l, m, n and use them
% to calculate mag for each and place it all into the new matrix
% which is of the same form as the data matrix.

% a,b are the coefficients of the expression in the form
% a*cos(t)+b*sin(t)

a = [x y*cy z*cz; data(2,1,1) data(2,1,2)*cy data(2,1,3)*cz;
      data(3,1,1) data(3,1,2)*cy data(3,1,3)*cz;
      data(4,1,1) data(4,1,2)*cy data(4,1,3)*cz]*lmn2xyz;
b = [0 -y*sy -z*sz; 0 -data(2,1,2)*sy -data(2,1,3)*sz;
      0 -data(3,1,2)*sy -data(3,1,3)*sz;
      0 -data(4,1,2)*sy -data(4,1,3)*sz]*lmn2xyz;

for I = 1:4,
      new(I,1,:) = sqrt(a(I,:).^2 + b(I,:).^2);
      new(I,2,:) = wrap(-atan2(b(I,:),a(I,:))*180/pi + data(I,2,1));
end

% Now for the unidirectional case:
else

for I = 1:4,
      new(I,1,:) = [0 sqrt(data(I,1,1)^2 + data(I,1,2)^2 + data(I,1,3)^2) 0];
      new(I,2,:) = [0 data(1,2,1) 0];
end

end % of unidirectional case
```

```
% Now, if the amplitudes of the cosines are negative, I need to increase
% the associated phase by 180.

for I = 1:4,
       for J = 1:3,
       if new(I,1,J) < 0
       new(I,1,J) = - new(I,1,J);
       new(I,2,J) = wrap(new(I,2,J)+180);
       end
       end
end

% Now, figure out the angles of the primary direction.

phi = atan2(xyz2lmn(3,2),xyz2lmn(3,1))*180/pi;
theta = atan2(sqrt(xyz2lmn(3,1)^2 + xyz2lmn(3,2)^2))*180/pi;

% all done!
```

Bibliography

Beranek, L. L. *Acoustics*. The Acoustical Society of America, 1954.

Von Békésy, G. *Experiments in Hearing*. McGraw-Hill, NY, 1960.

Cece, J. A. *Ear, Nose & Throat: The Middle Ear*. <http://www.ear-nose-throat.com/mid-ear.html>, 1997.

Davis, C. Q. and Freeman D. M. "Using Video Microscopy to Measure 3D Cochlear Motions with Nanometer Precision", *Abstracts of the Twentieth Midwinter Research Meeting*. Association for Research in Otolaryngology, St. Petersburg, Florida, 1995.

David, C. Q. *Measuring Nanometer, Three-Dimensional Motions with Light Microscopy*. Massachusetts Institute of Technology, 1997.

Goode, R. L., Ball G., and Nishihara, S. "Measurements of Umbo Vibration in Human Subjects–Method and Possible Clinical Applications", *The American Journal of Otology*, May 1993.

Guinan, J. J. and Peake, W. T. "Middle-ear Characteristics of Anesthetized Cats", *The Journal of the Acoustical Society of America*, May 1967, p. 1237-1261.

Gyo, K., Aritomo, H., and Goode, R. L. "Measurement of the Ossicular Vibration Ratio in Human Temporal Bones by Use of a Video Measuring System", *Acta Otolaryngol* (Stockh) 1987; 103: 87-95.

Johnson, L. K. *Using Computer Microvision to Characterize the Motions of a Microfabricated Gyroscope*. Massachusetts Institute of Technology, 1997.

Kaiser, P. *The Joy of Visual Perception*. "Point and Line Spread Functions" <http://www.egd.igd.fhg.de/~vh/Ergonomie/Opt_Wahrnehmung/psf.htm>. August, 1997.

Pickles, J. O. *An Introduction to the Physiology of Hearing*. Academic Press, London, 1988.

Rosowski, J. J., David, P. J., Donahue, K. M., Merchant, S. N., and Coltrera, M. D. "Cadaver Middle Ears as Models for Living Ears: Comparisons of Middle Ear Input Immittance", *Annals of Otology, Rhinology, and Laryngology*, May 1990.

4900-31